Air Force Institute of Technology

AFIT Scholar

Theses and Dissertations   Student Graduate Works

3-13-2008

Modeling of SBS Phase Conjugation in Multimode Step Index Fibers

Justin B. Spring

Follow this and additional works at: https://scholar.afit.edu/etd

Part of the Optics Commons

Modeling of SBS Phase Conjugation in Multimode Step Index Fibers

THESIS

Justin B. Spring, Captain, USAF

AFIT/GAP/ENP/08-M09

DEPARTMENT OF THE AIR FORCE
AIR UNIVERSITY

AIR FORCE INSTITUTE OF TECHNOLOGY

Wright-Patterson Air Force Base, Ohio

AFIT/GAP/ENP/08-M09

Modeling of SBS Phase Conjugation in Multimode Step Index Fibers

THESIS

Presented to the Faculty

Department of Engineering Physics

Graduate School of Engineering and Management

Air Force Institute of Technology

Air University

Air Education and Training Command

In Partial Fulfillment of the Requirements for the

Degree of Master of Science in Physics

Justin B. Spring, B.A.

Captain, USAF

March 2008

AFIT/GAP/ENP/08-M09

MODELING OF SBS PHASE CONJUGATION IN MULTIMODE STEP INDEX FIBERS

Justin B. Spring, B.A.

Captain, USAF

Approved:

Timothy H Russell	*13 MAR 2008*
Timothy Russell (Chairman)	Date
Salvatore Cusumano	*12 Mar 2008*
Salvatore Cusumano (Member)	Date
Kenneth Schepler	*12 Mar 2008*
Kenneth Schepler (Member)	Date

AFIT/GAP/ENP/08-M09

Abstract

Stimulated Brillouin scattering in a multimode step-index fiber can be used to generate a counter-propagating, phase-conjugate beam that would prove useful in many applications, such as near diffraction limited, double-pass high-power amplifiers or coherent beam combination. Relatively little modeling of such a fiber-based phase-conjugator has been done, making design decisions regarding type and length of fiber largely guesswork. A numerical model was constructed with the aim of providing educated predictions about the phase conjugate fidelity that could be expected from a given pump intensity input coupled into a specific fiber. A numerical perturbation algorithm was constructed to search for the Stokes modal arrangement with the highest gain for a given pump input. The gain was calculated from the differential equation for the Stokes power under the assumption that all pump/Stokes modes decay/grow at the same rate, and that the fiber was lossless. The model proves to be much more accurate in predicting experimentally observed phase conjugate fidelities than previous efforts. In addition, the phenomenon of beam cleanup to higher order fiber modes is predicted and explained.

Acknowledgements

Many people deserve my thanks for their valuable contributions to this effort. My advisor, Maj Tim Russell, was instrumental in providing an interesting topic to explore, as well as always providing timely and insightful answers to my many questions. The modeling work in this thesis closely mirrored experiments being performed by Maj Steve Massey, with whom I'm sure I exchanged hundreds of emails as we bounced ideas off one another. I know these conversations benefitted me greatly, I hope he feels the same.

My friends, those at AFIT and elsewhere, always provided a pleasant reminder that there is life outside of school. Tuesday nights and the month of March hold new meaning for me. My family was always there for me, whether it was a long conversation with Dad, joking with my brothers on the phone, escaping to sunny New Mexico for Christmas, or seeing pictures of my new niece Savannah, they always brought a smile to my face.

Lastly, this thesis is dedicated to my mother's memory. Her virtues were too numerous to list, much less in a sentence or two. Mom, I love you, and miss you terribly.

Justin B. Spring

Table of Contents

List of Figures

List of Tables

List of Symbols

x

Modeling of SBS Phase Conjugation in Multimode Step Index Fibers

I. Introduction

Lasers have found a myriad of applications since their initial experimental demonstration nearly 50 years ago [1]. Many of the most common laser commercial technologies involve relatively low power devices, milliwatts or less, that are used to etch optical storage media such as compact discs, or to scan barcodes in store checkout lines. High power lasers have also found use in industry for welding and cutting tasks. While the military has adopted lasers for tasks such as targeting and range-finding, stringent performance requirements have hampered their further integration. Most commercial lasers are either relatively low power or make significant sacrifices in beam quality, system weight, size, and complexity to achieve higher powers. While a poor quality beam delivered from a very heavy and large laser may be acceptable in an automobile factory where a controlled environment is available, and the laser only needs to propagate a very small distance to target, such a device would be unacceptable for most military uses.

Many defense applications simultaneously demand high power and good beam quality in a laser system with a minimal logistical footprint. The requirement for a high beam quality is rooted in the frequent need to propagate the beam through a significant distance to target. A low quality beam will have a significantly higher

divergence that will result in most of the light missing its intended destination. High output powers are required partly to account for the losses involved in long range propagation of even a near Gaussian laser beam, and even higher powers are needed if the laser is intended as a weapon at such ranges. Sadly, these demands for high power and good beam quality are usually countervailing. To understand why, one must understand the basics of laser operation.

Lasers are energy conversion devices. They convert energy from one source, whether it be from a chemical reaction, electricity, or even another laser, into coherent light of a well-defined wavelength that often exhibits a low angular divergence. While chemical lasers are the current focus of military systems, such as the Airborne Laser (ABL), due to the high powers they can provide, their complexity, size, and large logistical footprint have led investigators to search for alternatives. Solid-state and fiber lasers have attracted interest for their reduced maintenance requirements, but these operate at powers that are too low for military weapons-grade applications. To achieve high powers, a large amount of pump power must be introduced somewhere in the system, either in the lasing cavity or in an external amplifier. Since pumping is never a perfectly efficient process, some heat will be introduced, and for very high pump powers this heat can introduce prohibitively large thermal distortions to the beam profile in a solid state laser or amplifier.

In a fiber laser or amplifier, thermal aberrations are limited because the waveg-uide only permits a finite number of modes that, in general, cannot support the arbitrary thermal distortions introduced in a solid state device. However, while sin-

gle mode fibers are very common and easy to construct, they are generally not used for high power amplifiers because of their small core size. To permit higher powers, the core is typically enlarged to reduce the intensity below the threshold of damage and parasitic nonlinear effects. However, by enlarging the core, higher order modes are introduced and these modes will typically distort the input beam profile. While special designs, such as photonic crystal fibers, can increase the range of single-mode operation, there will still be an upper limit in core size at which good beam quality is lost. Thus, higher powers typically imply larger distortions to the beam profile, which will result in a much larger divergence to the beam and thus less power on target.

A phase conjugate mirror (PCM) can be used to maintain good beam quality despite the use of multimode fiber amplifiers, to name one of many potential applications. To learn what a phase conjugate mirror is, one can consider a 'probe' electric field:

$$\vec{E}_p(\vec{r}, t) = \frac{1}{2}\hat{A}(\vec{r})e^{i(\omega t - kz)} + c.c. \qquad (1.1)$$

where $\hat{A}(\vec{r})$ is the complex amplitude, which is a function of the spatial position $\vec{r}$ and contains both phase and polarization information, ω is the angular frequency, and $c.c.$ represents the complex conjugate of the first term. Now consider the wave equation in a linear, source-less medium:

$$\nabla^2 \vec{E}_p - \mu\epsilon(\vec{r})\frac{\partial^2 \vec{E}_p}{\partial t^2} = 0 \qquad (1.2)$$

where μ is the magnetic permeability, and $\epsilon(\vec{r})$ is the dielectric constant of the medium. If we break the Laplacian into transverse and longitudinal components, $\nabla^2 = \nabla_T^2 + \partial^2/\partial z^2$, and make the slowly varying envelope approximation (SVEA), whereby $\frac{\partial^2 \hat{A}(\vec{r})}{\partial z^2} \ll 2k \frac{\partial \hat{A}(\vec{r})}{\partial z}$, then one obtains:

$$\nabla_T^2 \hat{A}(\vec{r}) + (\omega^2 \mu \epsilon(\vec{r}) - k^2)\hat{A}(\vec{r}) + 2ik\frac{\partial \hat{A}(\vec{r})}{\partial z} = 0 \qquad (1.3)$$

Taking the complex conjugate of both sides does not change the validity of the equation, yielding:

$$\nabla_T^2 \hat{A}^*(\vec{r}) + (\omega^2 \mu \epsilon(\vec{r}) - k^2)\hat{A}^*(\vec{r}) - 2ik\frac{\partial \hat{A}^*(\vec{r})}{\partial z} = 0 \qquad (1.4)$$

One finds that this conjugated equation describes an electric field that is the complex conjugate of only the spatial portions of the probe field:

$$\vec{E}_c(\vec{r}, t) = \frac{1}{2}\hat{A}^*(\vec{r})e^{i(\omega t + kz)} + c.c. \qquad (1.5)$$

One immediately notices the relation between the probe field and its spatial conjugate:

$$\vec{E}_c(\vec{r}, t) = \vec{E}_p(\vec{r}, -t) \qquad (1.6)$$

that is, this spatial phase conjugate field acts like the probe field with time reversed [2]. Consider a laser that outputs a near Gaussian beam, which traverses an aberrating

4

medium. This medium could be nearly anything, from a multimode fiber amplifier to the atmosphere. If one used a phase conjugate mirror to generate the time reversed electric field at the far end of the aberrator, this field would be reflected backwards such that its phasefronts would exactly mimic those of the incident wave. That is, after a second pass through the aberrator, the original Gaussian beam profile would be restored. Specifically addressing the divergent demands for high power and good beam quality mentioned above, one can envision a low power Gaussian laser beam that transits an amplifier, increasing both power and distortions to the irradiance pattern. After amplification, the distorted beam can reflect off a PCM and transit back through the aberrator a second time with the aberrations introduced in the first pass being removed after this second pass. Thus, a high power Gaussian beam would be output.

Such a perfect 'time reversed' field would be of enormous value in a variety of applications beyond near distortionless amplifiers. These include beam combination, correction for atmospheric aberrations, tracking of moving objects, image processing, and novel laser cavity designs [3]. These applications all have obvious military utility. However, the focus of this thesis is not a specific application or scenario, but on modeling the performance of a multimode step index fiber as a PCM through Stimulated Brillouin scattering (SBS). Throughout this thesis, the focus will be on the internal workings of such an SBS PCM, not on the aberrator or the larger system design.

So far, the questions 'What?' and 'Why?' have been addressed. To answer the former, the discussion is focused on generating the spatial phase conjugate of an

incident electric field. Regarding the latter, such a field could solve a host of problems, though here we focus on near distortionless amplifiers that could provide a high power near Gaussian laser beam suitable for military applications. The question 'How?' has not yet been asked. Specifically, how does one construct a PCM with the properties described above? There are two primary nonlinear optics based methods.

Degenerate four-wave mixing (DFWM) acts like a real-time hologram to generate a phase conjugate beam [3]. A traditional hologram is formed when a reference beam is overlaid with a probe beam, resulting in an interference pattern which is recorded on a photographic film. When the film is developed and reilluminated by another reference beam, the probe beam is reproduced. The probe is often a reflection from an object, and so illuminating the holographic film will produce a virtual image of the object. In four wave mixing, three beams are overlaid on a nonlinear medium, one being the probe beam, and two other pump beams that propagate through the medium in opposite directions. Each of the pump beams interferes with the probe beam, creating an interference pattern that is, in turn, read out by the other pump beam in the form of the phase conjugate of the probe. While a normal hologram is permanently recorded on film, the interference pattern created by the probe and pump beams in four wave mixing will change in real time to consistently return the phase conjugate of an evolving probe.

Stimulated Brillouin scattering can also produce a phase conjugate reflection, and is the focus of this thesis. SBS occurs when pump photons scatter off lattice vibrations in a nonlinear medium. This can be visualized as the absorption of a pump

6
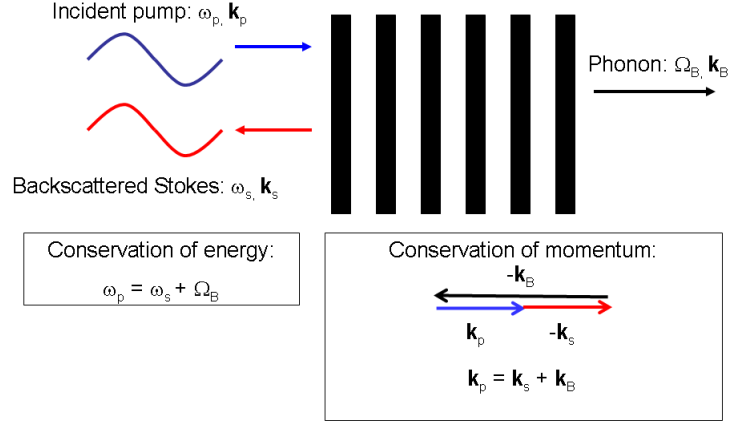
Figure 1.1. A schematic of SBS in a fiber. An incident pump photon scatters off a forward propagating lattice vibration, or phonon, leading to the creation of a slightly redshifted backscattered Stokes photon, and another phonon that increases the lattice vibration. This increase leads to a positive feedback loop, and nonlinear behavior.

photon, and the creation of a phonon and a lower frequency Stokes photon. The geometry of a fiber restricts this scattering to either the same direction in which the pump is propagating, or the reverse, backscattered case. However, forward scattering is prohibited by the phase matching condition, so SBS in a fiber is limited to backscattering, as seen in Figure (1.1). For each pump photon that scatters off the lattice vibrations, another phonon is created that reinforces these vibrations, leading to a positive feedback loop and a nonlinear increase in Stokes power after a certain threshold is passed.

It will be shown in the next chapter that the rate of growth of the Stokes beam is:

$$\frac{\partial I_s(r_\perp, z)}{\partial z} \propto I_s(r_\perp, z) I_p(r_\perp, z) \qquad (1.7)$$

where $I_s(r_\perp, z)I_p(r_\perp, z)$ represent the irradiance 'speckle' patterns of the incident pump and backscattered Stokes beams inside the multimode fiber. While the details will be left until later in this document, one can already qualitatively observe that, of the infinite number of possible Stokes configurations that could grow from spontaneous Brillouin noise, the $I_s(r_\perp, z)$ pattern that most closely matches the pump will give the largest product of intensities, and thus have the quickest growth. It is this irradiance overlap discrimination in the stimulated scattering process that forms the basis of an SBS PCM.

There are tradeoffs to consider when choosing whether to construct a DFWM or SBS PCM [3]. It is illustrative to consider these top level design concerns before delving into the details of a SBS PCM. A DFWM based mirror will give a phase conjugate beam that is of the same wavelength as the incident probe beam. Furthermore, there is no threshold power that must be crossed before the mirror will work, and for pump beams of sufficiently high power, the reflected phase conjugate can actually be of higher power than the incident probe. That is, a DFWM PCM can simultaneously serve as an amplifier. In fact, such amplifying DFWM PCMs have served as the basis of novel laser cavities which are so forgiving that they will lase with any moderately reflective surface nearby, including a metal spatula [3].

The alternative, an SBS device, has none of these advantages. The Stokes wave is of a slightly longer wavelength than the incident probe, and so even if a phase conjugate beam is formed, this beam will not be able to perfectly retrace the phase fronts of the pump. For short propagation distances this error is negligible, but this

effect usually precludes SBS PCM for applications such as correction of atmospheric aberrations. SBS also has a power threshold that must be crossed for the mirror to have an appreciable reflectivity, and this reflection coefficient will always be less than one, at least for the case of the passive, undoped silica fiber waveguides considered here. That is, an SBS PCM cannot simultaneously amplify.

With all the disadvantages previously mentioned, why would one ever resort to an SBS PCM? The short answer is that their design requirements are relatively simple [3]. All that is required is a nonlinear medium, of which there are many examples ranging from the compressed methane cell in which phase conjugate beams were first discovered [4], to solid silica fibers in which many modern experiments are performed, and a pump beam with enough power to exceed the SBS threshold. In contrast, DFWM requires three beams rather than one, and the two counterpropagating pump beams, which simultaneously form the interference pattern hologram and read it out, must have a high wavefront quality. Furthermore, the nonlinear medium in which the three beams are mixed must be of high optical quality. Suffice it to say, the choice of PCM will depend on the specific application, and one type is not inherently superior to the other.

The stage has now been set. The definition of a phase conjugate beam has been given in Equation (1.5), and a few of the many possible applications have been mentioned in passing, enough to justify why this is a topic worthy of research interest. The two methods for generating these beams, DFWM and SBS, have been discussed, with a presentation of the relative advantages and drawbacks of each.

Now that it is known how this thesis fits into the bigger picture, the focus can be narrowed to the research conducted here. Specifically, this thesis focuses on modeling continuous wave (CW) SBS phase conjugation in a multimode step index fiber, and predicting how the quality of the phase conjugate reflection (the fidelity) varies with fiber core size, length, the number of modes it supports, and the incident pump power.

While theoretical investigations of SBS PCMs have been conducted by a number of authors, the model constructed here offers new insights. A significant amount of theoretical work has been done on SBS PCM in a focused free space geometry, as opposed to the waveguide analyzed here [5, 6]. Waveguide SBS phase conjugation theory has attracted less interest, though there still have been some noteworthy efforts. Lehmberg implemented a numerical solution of a SBS waveguide PCM, though his treatment was limited to two dimensions and thus, while it was noteworthy for accurately matching theoretical predictions of earlier researchers, is not applicable in actually designing real world devices [7]. Hellwarth devised one of the earliest theoretical treatments of SBS phase conjugation in a waveguide, and concluded his article with a prediction of the phase conjugate fidelity that could be obtained for a given waveguide size and length [8]. While his results are significant and are one of the most referenced works on this subject, they suffer from several limitations. These include the lack of consideration for any pump depletion, and the use of perturbation theory with a perfect phase conjugate starting point.

It will be shown later that the quality of the phase conjugate reflection from a given fiber increases as the fiber is shortened. Unfortunately, the SBS threshold

will also increase, meaning more power is required to generate a backscattered Stokes beam. This obviously means that some tradeoff between the two variables must take place. While SBS threshold in fibers is a well-studied topic, making predictions about phase conjugate quality as a function of fiber length is very haphazardous, with current models, such as Hellwarth, vastly understating the lengths required for a given fidelity. This would imply very high threshold powers, and make device construction impractical, which is not observed experimentally. This thesis was an attempt to bridge this gap between theory and experiment.

The model described in this thesis is a full three dimensional analysis of a step index multimode fiber, where consideration for pump depletion effects is included and compared to the no pump depletion case. The eventual aim of the model is to give accurate predictions of how fiber type, length, and input pump power will affect the performance of a step index multimode fiber PCM. This could be a valuable tool in the hands of experimentalists and system developers attempting to make informed decisions on design choices. Chapter 2 lays a more detailed framework of the theory required in the construction of the model, including a description of the allowed modes in a fiber and the origins of the SBS coupled differential equations describing the changes in the pump and Stokes irradiances in the fiber and how these forms can lead to a phase conjugate reflection. Chapter 3 moves from general theory into the specifics of how the model works, the different categories of solutions that were considered and what assumptions were made for each of these solutions. Chapter 4 moves on to the results obtained from the model, and a discussion of how these results

factor into experimental results and previous theoretical predictions. Chapter 5 ends with a suggestion for future work and conclusions.

II. General Theory

Foundational Theory

The first step in modeling an SBS phase conjugate mirror in an optical fiber is to model the multimode fiber itself. An incident field can be constructed from an arbitrary linear combination of a finite number of fiber modes. After calculation of the various propagation constants, each mode can be independently propagated down the fiber. Knowledge of these propagation constants, along with the initial percentage of power in each mode, allows a calculation of the irradiance distribution at any given longitudinal distance down the fiber. Once this three-dimensional irradiance distribution for the pump has been found, one can estimate the gain for a phase conjugate Stokes beam produced through SBS. This SBS gain is a function of the spatial overlap between the irradiance distribution of the Stokes and the pump. This overlap will gradually degrade over the length of the fiber due to the multiple modes present and the frequency shift inherent to SBS. Determining how the gain of the phase conjugate form of the Stokes beam depends on input pump power and fiber length forms the heart of this thesis.

Optical fibers confine light through total internal reflection due to the higher index of refraction in their core relative to the neighboring cladding, as seen in Figure
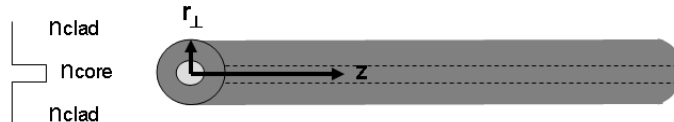
Figure 2.1.   Schematic of a step index fiber, with the indices of refraction in the core and cladding shown on the left, and the coordinate system specified in the fiber.

13

(2.1). However, multiple restrictions are placed on the fields inside such dielectric waveguides. They must satisfy Maxwell's equations:

$$\nabla \times \vec{E} = -\mu_0 \frac{\partial \vec{H}}{\partial t} \tag{2.1}$$

$$\nabla \times \vec{H} = \frac{\partial \vec{D}}{\partial t} \tag{2.2}$$

$$\nabla \cdot \vec{D} = 0 \tag{2.3}$$

$$\nabla \cdot \vec{H} = 0 \tag{2.4}$$

which, in the form above, describe the nonmagnetic and source free environment found in a typical fiber. The magnetic and electric fields, $\vec{H}$ and $\vec{E}$, as well as the magnetic flux density and electric displacement, $\vec{B}$ and $\vec{D}$, are related by the constitutive relations:

$$\vec{D} = \varepsilon_0 \vec{E} + \vec{P} = \varepsilon \vec{E} \tag{2.5}$$

$$\vec{B} = \mu_0(\vec{H} + \vec{M}) = \mu \vec{H} \tag{2.6}$$

where $\vec{P}$ and $\vec{M}$ represent the induced dipole and magnetic moment per unit volume respectively, and the final equality in the constitutive relations applies in linear, isotropic materials. Taking the curl of Equation (2.1), plugging in Equations (2.2), (2.3) and the linear, isotropic form of (2.5) leads one to the linear wave equation:

$$\nabla^2 \vec{E} - \left(\frac{n}{c}\right)^2 \frac{\partial^2}{\partial t^2} \vec{E} = 0 \tag{2.7a}$$

14

$$\nabla^2 \vec{E} = \nabla_T^2 \vec{E} + \frac{\partial^2 \vec{E}}{\partial z^2} = \frac{1}{r} \frac{\partial}{\partial r} \left(r \frac{\partial \vec{E}}{\partial r} \right) + \frac{1}{r^2} \frac{\partial^2 \vec{E}}{\partial \theta^2} + \frac{\partial^2 \vec{E}}{\partial z^2} \tag{2.7b}$$

where n is the index of refraction, $n/c = \sqrt{\mu_0 \varepsilon}$ in this nonmagnetic fiber, and Equation (2.7b) gives the Laplacian in the cylindrical coordinates that are appropriate for the optical fibers analyzed in this thesis. Note that the Laplacian can be broken out into its transverse, ∇_T^2, and longitudinal, $\frac{\partial^2}{\partial z^2}$, components. Equation (2.7a) is applicable to each of the three scalar components of the electric field vector, $\hat{r}, \hat{\theta}$ and $\hat{z}$, though the unit vectors in the $\hat{r}$ and $\hat{\theta}$ directions are not constant in space, leading to a coupling of the three component wave equations when the Laplacian is taken [9]. While solutions can still be found for a step index fiber, the analysis is considerably easier if the weakly guiding approximation is made, namely that:

$$n_{core} - n_{clad} \ll 1 \tag{2.8}$$

where the indices apply in the regions labeled by the subscripts. Using this approximation, only paraxial fiber modes, those propagating nearly parallel to the fiber axis, will remain trapped. The longitudinal components of the electric and magnetic fields are then very weak, and the guided modes are nearly transverse electromagnetic (TEM) [9].

Previously, the polarization of the mode could have been a combination of all three Cartesian components but, in the weakly guiding approximation, the longitudinal component can be neglected, considerably reducing the complexity. While a de-

tailed analysis is beyond the scope of the introductory treatment here, the transverse electromagnetic (TEM) field that remains after neglecting the longitudinal polarization will be linearly polarized in the weakly guiding fibers discussed here. Anticipating this linear polarization, the electric field will be decomposed into its Cartesian polarization components $\hat{x}, \hat{y}, \hat{z}$, though the spatial dependence of these components, to include the Laplacian, is still written in the cylindrical form given in Equation (2.7b) due to the geometry imposed by the fiber [10]. One can then re-express Equation (2.7a) in scalar form for any one of the Cartesian components of the electric field, however only the two transverse components will be significant. Furthermore, as the modes in this weakly-guiding fiber are linearly polarized, the entire electric field can be described through a solution of Equation (2.7a) in one Cartesian direction [11].

Maxwell's equations impose the boundary condition that the tangential components of $\vec{E}$ must be continuous across the core-cladding dielectric interface. This restriction, along with the limitation on propagation angles that preserves total internal reflection, allows only certain field distributions, or modes, to exist inside the waveguide. We look for linearly polarized modal distributions that propagate down the fiber with the scalar form:

$$E = E(r, \theta) = R(r)\Theta(\theta)\exp[i(\beta z - \omega t)] \tag{2.9}$$

where $R(r)$ and $\Theta(\theta)$ express the radial and azimuthal field dependence respectively, and β is the propagation constant of the fiber mode. Inserting Equation (2.9) into

16

the scalar form of Equation (2.7a), allows one to easily determine the azimuthal dependence through separation of variables, yielding the result:

$$\Theta(\theta) = \exp[i\ell\theta] \tag{2.10}$$

where ℓ is an integer. Substituting this azimuthal dependence into Equation (2.9) and the result into the scalar form of Equation (2.7a), while making use of the cylindrical coordinate Laplacian in Equation(2.7b), yields:

$$\left(\nabla_T^2[R(r)\Theta(\theta)] - \left(\beta^2 - \left(\frac{n\omega}{c}\right)^2\right)R(r)\Theta(\theta)\right)exp[i(\beta z - \omega t)] = 0 \tag{2.11a}$$

$$\frac{\partial^2 R(r)}{\partial r^2} + \frac{1}{r}\frac{\partial R(r)}{\partial r} - \left(\frac{\ell^2}{r^2} + \beta^2 - \left(\frac{n\omega}{c}\right)^2\right)R(r) = 0 \tag{2.11b}$$

where, in moving from Equation (2.11a) to (2.11b), the transverse Laplacian has been evaluated and the result divided by $\Theta(\theta)exp[i(\beta z - \omega t)]$. Through a non-weakly guiding analysis, one can show that in general:

$$n_{core}k_0 > \beta > n_{clad}k_0 \tag{2.12}$$

where $k_0 = \frac{2\pi}{\lambda_0}$ and λ_0 is the free space wavelength [9]. In a step index fiber, it is then convenient to define two new propagation constants:

$$k_T^2 = n_{core}^2 k_0^2 - \beta^2 \tag{2.13}$$

17

$$\gamma^2 = \beta^2 - n_{clad}^2 k_0^2 \tag{2.14}$$

where it will be found that k_T is the propagation constant in the transverse plane. By separately writing Equation (2.11b) in the core and clad regions and including Equations (2.13) and (2.14) in the appropriate regions, one can write:

$$\frac{\partial^2 R(r)}{\partial r^2} + \frac{1}{r}\frac{\partial R(r)}{\partial r} + \left(k_T^2 - \frac{\ell^2}{r^2}\right)R(r) = 0, \quad r < a \quad \text{(core)} \tag{2.15a}$$

$$\frac{\partial^2 R(r)}{\partial r^2} + \frac{1}{r}\frac{\partial R(r)}{\partial r} - \left(\gamma^2 + \frac{\ell^2}{r^2}\right)R(r) = 0, \quad r > a \quad \text{(clad)} \tag{2.15b}$$

where a is the radius of the step index fiber core. These are well-known differential equations whose solutions are Bessel functions [12]. By restricting the solutions to remain finite at $r = 0$ and as $r \longrightarrow \infty$, the solution for the radial dependence of the electric field can be expressed as:

$$R(r) = \begin{cases} C_\ell J_\ell(k_c r) & r < a \quad \text{(core)} \\ \\ D_\ell K_\ell(\gamma r) & r > a \quad \text{(clad)} \end{cases} \tag{2.16}$$

where J_ℓ and K_ℓ are the ℓth order Bessel and modified Bessel functions respectively, and C_ℓ and D_ℓ are constants whose value depends on the power in the ℓth mode [13].

In the weakly guiding case where the electric field is linearly polarized, both the normal and tangential components must be continuous across the core-clad interface [10]. Maxwell's equations impose boundary conditions such that the tangential component of the electric field must always be continuous at an interface. Using

18

Equation (2.3) in a linear material, one can implement the divergence theorem to see that the normal component of the electric displacement, $\vec{D}$, is continuous across the interface. However, in the weakly guiding case, the indices of refraction, and thus the permittivities, of the core and cladding are almost the same. Since $\vec{D} = \epsilon\vec{E}$, the weakly guiding case lets us approximate the continuity of the normal component of $\vec{D}$ with the continuity of the normal component of $\vec{E}$.

By inspection, the azimuthal and longitudinal dependence will satisfy this interface continuity boundary condition. Performing a more detailed analysis on each of the Cartesian electric and magnetic field components would show that their continuity is equivalent to the continuity of $R(r)$ and $\partial R/\partial r$ at the core-clad boundary [9]. Using known properties of the derivatives of Bessel functions, this gives the characteristic equation:

$$X\frac{J_{\ell\pm1}(X)}{J_\ell(X)} = \pm\sqrt{V^2 - X^2}\frac{K_{\ell\pm1}(\sqrt{V^2 - X^2})}{K_\ell(\sqrt{V^2 - X^2})}, \tag{2.17}$$

where $X = k_T a$ and $V = 2\pi\frac{a}{\lambda_0}\sqrt{n_{core}^2 - n_{clad}^2}$ [12].

In the work to be done, the wavelength λ_0 and fiber parameters, n_{core}, n_{clad}, and a will be known, enabling a calculation of V. Choosing a value of ℓ gives a family of linearly polarized modes, $LP_{\ell m}$, where m takes integer values from 1 up to the maximum number of modes allowed for the given ℓ. The corresponding propagation constants are determined by solving Equation (2.17) transcendentally for X which, using Equation (2.13), leads to β.

The above analysis is important because it provides, for a given random multimode input, the irradiance distribution throughout the fiber. This is critical in determining the SBS gain. SBS is a third order nonlinear interaction, whereby an incident pump photon scatters off a retreating density variation, producing a red-shifted Stokes photon and a phonon. In the above derivation of the functional form of the fiber modes, a linear material was assumed in writing Equation (2.7a). While the small core size greatly increases the irradiance inside these fibers, it simultaneously drastically decreases the interaction length in the transverse direction for nonlinear processes, essentially making these linear materials in this transverse dimension.

As we turn to the long distances that are possible along the fiber's longitudinal direction, this interaction length is no longer restricted and nonlinear effects become important. In this latter case, we must re-write Equation (2.7a), where one now includes the nonlinear polarization and as such $\vec{D} \neq \epsilon \vec{E}$. The following development closely follows that presented in Equations (1.1)-(1.3), except now the nonlinear polarization term is included. If one expresses the polarization in Equation (2.5) as $\vec{P} = \epsilon_0 \chi^{(1)} \vec{E} + \vec{P}_{NL}$, and considers the frequency domain where $\vec{E}(\vec{r}, t) = \int_{-\infty}^{\infty} \vec{E}(\vec{r}, \omega) e^{-i\omega t} d\omega$ (and similarly for $P(\vec{r}, t)$), then the nonlinear wave equation can be derived from Maxwell's equations (as shown for Equation (2.7a)) to give:

$$\nabla^2 \vec{E}(\vec{r}, t) = -\mu_0 \frac{\partial^2 \vec{D}(\vec{r}, t)}{\partial t^2}$$

$$\nabla^2 \vec{E}(\vec{r}, \omega) + \frac{\omega^2}{c^2} \epsilon_L(\omega) \vec{E}(\vec{r}, \omega) = -\mu_0 \omega^2 \vec{P}_{NL}(\vec{r}, \omega) \tag{2.18}$$

20

where $\epsilon_L(\omega) = 1 + \chi^{(1)}$ describes the portion of $\vec{D}$ that is linearly dependent on the electric field [14]. Again breaking the Laplacian into longitudinal and transverse components, making the slowly varying envelope approximation, and expressing $\vec{E}(\vec{r}, \omega) = \hat{E}^\omega(r, \theta, z)e^{i\beta z}$, we find that:

$$\left[\nabla_T^2 \hat{E}^\omega(r, \theta, z) + 2i\beta \frac{\partial \hat{E}^\omega(r, \theta, z)}{\partial z} - \beta^2 \hat{E}^\omega(r, \theta, z) + \frac{\omega^2}{c^2}\epsilon_L(\omega)\hat{E}^\omega(r, \theta, z) \right] e^{i\beta z}$$

$$= -\mu_0 \omega^2 \vec{P}_{NL}^\omega \tag{2.19}$$

where the z dependence in $\hat{E}_i^\omega(r, \theta, z)$ is due to the overall growth or decay of the electric field as it propagates along the fiber, and the much more rapid phase oscillations of the field, $e^{i\beta z}$, have been factored out.

One can simplify Equation (2.19) by going back and re-writing Equation (2.11a) such that transverse terms are combined into the $E(r, \theta)$ defined in Equation (2.9), to give:

$$\nabla_T^2 E(r, \theta) - \left(\beta^2 - \left(\frac{n\omega}{c} \right)^2 \right) E(r, \theta) = 0 \tag{2.20}$$

where it is noted that $n^2 = \epsilon_L$. At first glance, the electric field terms in Equations (2.19) and (2.20) do not appear to match. However, this is only because the $\hat{E}^\omega(r, \theta, z)$ term takes a more general form than was necessary for the $E(r, \theta)$ that was used previously. However, these generalizations do not hinder the use of Equation (2.20) in cancelling the first, second and fourth terms in Equation (2.19). The field $E(r, \theta)$ was written assuming a linearly polarized, monochromatic field with no

21

power growth or decay in the z direction. The superscript ω in $\hat{E}^\omega(r, \theta, z)$ defines this as the monochromatic contribution of frequency ω to a more generalized polychromatic field, and if we again restrict ourselves to linear polarization then we can write this more generalized field in scalar form $E^\omega(r, \theta, z)$. In addition, the three terms in Equation (2.19) that cancel each other out involve the electric field multiplied by a constant term, or derivatives with respect to the transverse coordinates, not z. Thus, the slowly-varying z dependence in the $\hat{E}^\omega(r, \theta, z)$ term can be separated out and, Equation (2.20) can be used to cancel the first, second and fourth terms of Equation (2.19).

These terms cancel each other because we solved for the modal propagation constants β such that this would hold true. Making this simplification to Equation (2.19), and now decomposing the total field into the contributions from various fiber modes labeled by i, the nonlinear wave equation is further simplified to:

$$\sum_i \frac{\partial \hat{E}_i^\omega(r, \theta, z)}{\partial z} e^{i\beta_i z} = \frac{i\mu_0 \omega^2}{2k} \vec{P}_{NL}^\omega \qquad (2.21)$$

where k is the average value of the modal propagation constants β_i. Taking this average is a good approximation because these values are relatively closely spaced, and the small differences are most significant when in a phase term such as $e^{i\beta_i z}$.

To proceed further, we must solve for the nonlinear polarization, P_{NL}, induced by SBS. This effort starts by invoking the general principles of energy and momentum conservation, in this case where an incident pump photon produces a phonon and a

22

backscattered Stokes photon, yielding the relations previously seen in Figure (1.1):

$$\omega_p = \omega_s + \Omega_B \tag{2.22a}$$

$$\vec{k}_p = \vec{k}_s + \vec{k}_B \tag{2.22b}$$

where the subscript p represents the incident pump, s represents the backscattered Stokes, and B indicates the acoustic Brillouin phonon. There is a positive feedback loop evident in Equations (2.22), whereby the scattering of the pump off the sound wave increases the Stokes output, and the interference of the Stokes and pump has a frequency component that matches, and reinforces, this same sound wave. In a quantum description, for each pump photon that is annihilated a phonon and counterpropagating Stokes photon are created, with the phonon reinforcing the sound wave that initially caused the scattering. Under appropriate conditions, this feedback can lead to exponential growth in the Stokes wave [14].

In the fiber, there is a coupling between phonons and photons. The previous discussion of SBS took a quantum view of the scattering process. This is valid in some related processes, such as Raman scattering, which involves the vibrational modes within a single molecule, however Brillouin scattering arises from a distributed lattice vibration that is described by the offset of one atom or molecule relative to its neighbors [15]. Due to this distributed effect throughout the lattice, traditionally one analyzes SBS more quantitatively by favoring a classical approach over the quantum view introduced above.

One must find a way to relate the density variations that create the phonon to the electromagnetic energy in the photons. This is accomplished by equating the work done to compress a material with the change in electromagnetic field energy due to a change in its density, and thus permittivity. Proceeding in this manner, one can find the electrostrictive pressure induced by an electromagnetic field:

$$<p_{st}>= -\frac{1}{2}\,\gamma_e <|E|^2>$$ (2.23)

where γ_e is the electrostrictive constant which describes how much the permittivity changes for a given density change, and the brackets indicate a time average [14]. This pressure is then used as the source term in the acoustic wave equation, which is not shown in this cursory look at the SBS polarization derivation. Making the slowly varying envelope approximation (SVEA), one can analytically determine the density variation in the fiber as a function of the material and electric field characteristics. This density change gives rise to a permittivity change, which induces a nonlinear polarization that is substituted into Equation (2.21). This nonlinear polarization then couples the pump and Stokes fields together.

The specific terms in this nonlinear polarization, found by the method outlined above, are not of immediate interest to the research conducted here and are largely absorbed into the Brillouin gain mentioned below. However, it is worth noting that

the SBS-induced polarization at the Stokes frequency will be proportional to:

$$\vec{P}_{NL-\omega_s} \propto (\vec{E}_p^* \cdot \vec{E}_s)\vec{E}_p \tag{2.24}$$

This implies that the differential equation describing the Stokes growth, Equation (2.21), can be written:

$$\frac{\partial \vec{E}_s(\vec{r})}{\partial z} \propto (\vec{E}_p^* \cdot \vec{E}_s)\vec{E}_p \tag{2.25}$$

where all the modal amplitudes $\hat{E}_i$ have been absorbed into the total electric field $\vec{E}$. By multiplying Equation (2.25) by $\vec{E}_s^*$, and adding the resulting equation to its complex conjugate, one can put the differential equation entirely in terms of irradiances. After pursuing a similar strategy for the wave equation at ω_p, one can write, for a counterpropagating Stokes near resonance:

$$\frac{\partial I_p(r_\perp, z)}{\partial z} = -g(r_\perp)\frac{\omega_p}{\omega_s}I_p(r_\perp, z)I_s(r_\perp, z) - \alpha_p I_p(r_\perp, z) \tag{2.26a}$$

$$\frac{\partial I_s(r_\perp, z)}{\partial z} = -g(r_\perp)I_p(r_\perp, z)I_s(r_\perp, z) + \alpha_s I_s(r_\perp, z) \tag{2.26b}$$

where $g(r_\perp)$ represents the Brillouin gain as a function of transverse position within the fiber and serves as the proportionality constant that was left out above, and I and α represent the irradiance and loss, respectively, in the appropriate beams. The loss term was not included in the nonlinear wave equation, but can be added in at the end as real waveguides always have a nonzero loss. It is worth noting here that the focus of this thesis is step index fibers, where $g(r_\perp)$ assumes two values, one in

25

the core and another in the cladding, with the former value being assumed as the remaining analysis focuses on modes within the fiber core.

One can write the electric field distribution of either pump or Stokes beam in terms of a set of orthonormal fiber modes:

$$E_{p,s}(r_\perp, z, t) = \sum_f A_{p,s}^f(z) \psi_{p,s}^f(r_\perp) \cos\left(\beta_{p,s}^f z - \omega_{p,s} t + \phi_{p,s}^f\right) \qquad (2.27)$$

where the summation is over all the modes allowed by the fiber, and the specific mode formerly described by ℓ and m is now described, for simplicity, by a single superscript f. The term $\psi_{p,s}^f(r_\perp)$ includes both the radial and azimuthal dependence described in Equation (2.9), $\phi_{p,s}^f$ is an overall modal phase factor, and the amplitude of each mode, $A_{p,s}^f(z)$, is now a function of distance down the fiber due to possible SBS gain and fiber loss [16]. These modes are labeled orthonormal because the radial and azimuthal dependence of Equations (2.16) and (2.10) gives a $\psi(r_\perp)$ that, upon proper normalization, has the property:

$$\int \psi^a(r_\perp) \psi^b(r_\perp) dA = \delta_{ab} \qquad (2.28)$$

where δ_{ab} is the Kronecker delta. In addition, the starting amplitudes are normalized such that:

$$\sum_i A_i^2(0) = 1 \qquad (2.29)$$

26

It is then straightforward to write the corresponding intensity distributions with such an electric field:

$$I_{p,s}(r_\perp, z) = 2\varepsilon_0 cn\langle E_{p,s}(r_\perp, z, t)^2\rangle$$

$$= \varepsilon_0 cn \sum_{f,q} A^f_{p,s}(z) A^q_{p,s}(z) \psi^f_{p,s}(r_\perp) \psi^q_{p,s}(r_\perp) \cos\left(\Delta\beta^{fq}_{p,s} z + \Delta\phi^{fq}_{p,s}\right) \quad (2.30)$$

where the brackets indicate a time average that eliminates terms oscillating at 2ω, ε_0 is the permittivity of free space, c is the speed of light, and n is the index of refraction of the core. Included are new terms representing the difference in longitudinal propagation constants and modal phases, given by:

$$\Delta\beta^{fq}_{p,s} = \beta^f_{p,s} - \beta^q_{p,s}$$

$$\Delta\phi^{fq}_{p,s} = \phi^f_{p,s} - \phi^q_{p,s} \quad (2.31)$$

Equation (2.26b) must be solved to determine either the effective gain or back-reflected power for a certain Stokes configuration. Given that many modern fibers have very low loss, the main term of interest in Equation (2.26b) is the product of intensities, $I_p(r_\perp, z)I_s(r_\perp, z)$. For the multimode fibers investigated in this thesis, it is necessary to express the pump and Stokes intensities as shown in Equation (2.30). The z dependence in this intensity resides in both the cosine phase terms, and in the amplitude $A_{p,s}(z)$. The cosine terms present no difficulty, as the propagation constants can be determined by the methods outlined above, and the modal phase

offset terms are constants, which usually take a known set of values depending on the modal configuration being analyzed.

The longitudinal dependence of the amplitude, however, is much more complicated. In reality, each mode of the pump and Stokes can grow or decay at a different rate. However, these rates of change are not independent of one another, but coupled together. For example, if the incident pump is largely in the fundamental LP_{01} mode, the backscattered Stokes will favor a high growth for its LP_{01} content, which, in turn, will lead to a more rapid decrease of the pump's fundamental mode due to depletion effects. Furthermore, coupling effects arise that allow higher order pump modes, such as the LP_{02} or LP_{11}, to alter the growth of the Stokes LP_{01} mode. One can easily see how complicated this problem can become, and further detail is included in the next section.

To greatly simplify the analysis, the rest of the work presented in this thesis assumes that all the modes of either the pump or Stokes change at the same rate down the fiber:

$$A_{p,s}^f(z) = \kappa_{p,s}(z) A_{p,s}^f(0) \tag{2.32}$$

where $\kappa_{p,s}(z)$ represents this common rate of change for either the pump or Stokes beam, and $A_{p,s}^f(0)$ represents the amplitude of mode f at the pump input end of the fiber, where $z = 0$. As mentioned above, in reality each mode can grow at a different rate, so this simplification introduces some error. However, attempting to include a more rigorous approach would greatly complicate the analysis, with the introduc-

tion of a boundary value problem involving a set of coupled differential equations. Related modeling efforts of SBS phase conjugation in the focused geometry, that is without a waveguide, encountered great difficulty in attaining a stable solution with this approach [17]. The solutions that were reached eventually resorted to significant simplifications and/or special launching conditions anyways. By assuming Equation (2.32) holds true, these significant pitfalls are avoided in the construction of an initial model. As will be shown later in this thesis, even with the common modal longitudinal change simplification, this model predicts experimental trends much more accurately than previous efforts. When discrepancies are observed between experiment and the model, a quantitative explanation is given for why these errors are rooted in the simplification of Equation (2.32).

With this common longitudinal change assumption, one can write out the full modal dependence of the $I_p(r_\perp, z)I_s(r_\perp, z)$ term in Equation (2.26b):

$$I_p(r_\perp, z)I_s(r_\perp, z) \propto \sum_{f,q,j,\nu} A_{ppss}^{fqj\nu} \kappa_p(z)^2 \kappa_s(z)^2 \psi_{ppss}^{fqj\nu}(r_\perp) \times$$

$$\cos(\Delta\beta_p^{fq} z + \Delta\phi_p^{fq}) \cos(\Delta\beta_s^{j\nu} z + \Delta\phi_s^{j\nu}) \qquad (2.33)$$

where the new variables are shorthand to describe the initial amplitudes and the transverse spatial dependence:

$$A_{ppss}^{fqj\nu} = A_p^f(0)A_p^q(0)A_s^j(0)A_s^\nu(0)$$

$$\psi_{ppss}^{fqj\nu}(r_\perp) = \psi_p^f(r_\perp)\psi_p^q(r_\perp)\psi_s^j(r_\perp)\psi_s^\nu(r_\perp) \tag{2.34}$$

Solving Equation (2.26b) is now a more tractable problem, but it still has not been specified what exact form $\kappa_{p,s}(z)$ will take. There are multiple approaches to this question, of varying complexity and physical authenticity, which form the basis for the different categories of solutions found in the following chapters.

Comparisons to Previous Work

A significant amount of work has been done on SBS phase conjugation since its discovery in 1972 [4]. Much of the early research was done in the former Soviet Union and focused on phase conjugation in the 'focused geometry,' which implies a waveguide was not used. Rather, an incident aberrated beam was focused down to a small spot, with a correspondingly high intensity, inside a nonlinear medium such as a compressed gas. In principle, these devices are very similar to the silica fiber phase conjugators discussed here, but the interaction length in this focused geometry is relatively short, forcing very high intensities to reach SBS threshold. Thus, pulsed systems were typically used in the early days to meet these requirements. From a modeling perspective, Equation (2.19) takes a different simplified form when a

waveguide is no longer used. There are no waveguide modes, so the summation over i is dropped, and the third and fourth terms cancel each other out as $\beta^2 = \epsilon_L \frac{\omega^2}{c^2}$. However, unlike before, the transverse Laplacian remains, complicating the analysis. There are excellent summary articles of this early, and extensive, work and further mention will not be made here [18].

In the literature of SBS phase conjugation in waveguides, there have been seemingly contradictory results. Most authors see a clear reduction in the quality of the backscattered phase conjugate Stokes as the fiber is lengthened [19]. This reduction in conjugate quality is due to the small wavelength shift of the Stokes relative to the pump, which gives an increasingly large phase error between the two as the fiber is lengthened. Where good phase conjugation has been observed in longer step-index fibers, it has been traced directly to a short coherence length of the pulsed pump, which will severely restrict the nonlinear interaction length in the fiber, making the physical length of the fiber largely irrelevant [20].

A quantitative analysis of the inverse relationship between the phase conjugate fidelity and waveguide length was conducted by Hellwarth, in one of the most cited theoretical works on the subject [8]. Starting with Equation (2.25), one can re-express all of the electric fields in terms of their constituent modes. Then, by multiplying both sides by $\psi^m(r_\perp)$ and integrating over the transverse dimensions, one can use Equation (2.28) to eliminate all but the mth term on the left side of Equation (2.25). This strategy is very similar to 'Fourier's Trick' which is used to isolate a single Fourier series coefficient. Returning to the result of the transverse integration, this makes the

31

longitudinal integration in the z direction trivial on the side of the equation without a summation, leaving the proportionality:

$$A_s^m \propto \sum_{ijn} A_{pps}^{ijn} \int_{area} \psi_{ppss}^{ijnm} dr_\perp \int_0^L e^{i(\beta_s^m + \beta_p^i - \beta_p^j - \beta_s^n)z} dz \qquad (2.35)$$

where the constants of proportionality have been left out for simplicity here, but are included in Hellwarth's analysis. Hellwarth rationalizes the omission of the majority of the terms in the triple summation by noting that the integral over the complex exponential often goes to zero, a realization that was independently reached in the construction of the model for this thesis. He then uses stationary perturbation theory on the remaining terms to solve the resulting coupled, linear differential equations to find the Stokes amplitudes A_s^m.

He examines a number of special cases, such as the perfect phase conjugate, or a Stokes form where every mode is excited equally but has an arbitrary phase term. However, he eventually concludes that the phase conjugate form of the Stokes will have a significantly higher gain than other possible modal permutations as long as the waveguide is short enough to satisfy:

$$L \leq 6r_0^{1/2} \frac{S}{N\Delta\lambda} \qquad (2.36)$$

where L is the length of the waveguide, S is the area of the waveguide, N is the number of excited modes, $\Delta\lambda$ is the wavelength separation between pump and Stokes, and

r_0 is the nonconjugated fraction of the backscattered power. Note that in Equation (2.36), N indicates the total number of modes, including both transverse polarization components. An r_0 value of 0 indicates a perfect phase conjugate, while a value of 1 would indicate no phase conjugate content. Later in this thesis, there will be plots of the phase conjugate fidelity, F, where $F = 1 - r_0$.

Several caveats must be made before applying Equation (2.36) arbitrarily. It was derived with a rectangular waveguide and equally excited modes in mind. Neither case holds for the silica fibers in this thesis. However, as long as the area is calculated with the correct formula, the S term poses no problems. The assumption that there are N equally excited modes is more troublesome. Hellwarth states his belief that the inequality can be applied even for unequally excited modes with arbitrary phase, as long as r_0 remains small, though he does not go into details on the justification. This leads to the final applicability warning, Hellwarth's entire analysis, by using perturbation theory, quickly loses predictive value as the nonconjugated perturbation grows larger. What values of r_0 are prohibitively large is also not clear. Despite these shortcomings, Hellwarth's inequality remains a valuable asset in making rough estimates of the tradeoff space between the multiple variables involve in SBS phase conjugate waveguide devices.

By substituting in the area of a circle for S, re-expressing $\Delta\lambda$ in terms of Ω_B, and putting the number of modes in terms of the fiber's numerical aperture, $N \approx$

$2(\frac{\pi a (NA)}{\lambda})^2$, Equation (2.36) can be written:

$$L \leq \frac{6 r_0^{1/2} c}{\Omega_B (NA)^2} \qquad (2.37)$$

where NA is the fiber's numerical aperture. As an example, if one wants an 80% phase conjugate Stokes beam with a 1064 nm source serving as the pump, and a 0.13 NA fiber is acting as the nonlinear medium, Equation (2.37) predicts the fiber length must be no longer than 0.47 meters. The Stokes shift in silica is given by $\frac{\Omega_B}{2\pi} = 16$ GHz. Keeping the same parameters, but switching to an extremely low NA of 0.06 only relaxes the length requirement to 2.22 meters. Russell used a lowest versus highest order mode acceptable phase error approach to reach the relation [16]:

$$L \leq \frac{2 n_{core} c \Delta \phi}{\Omega_B (NA)^2} \qquad (2.38)$$

where $\Delta \phi$ is the phase error. If one plugs in $\Delta \phi = \frac{\lambda}{10}$, $n_{core} = 1.48$, and uses a 0.13 NA fiber, a maximum length of 0.33 meters is obtained. If true, these limitations would severely hamper the applicability of fibers in making phase conjugate reflectors, as very high input powers would be required to excite SBS in such a short interaction length.

This thesis can be thought of as an attempt to produce a more accurate prediction of the tradeoff between fiber length and phase conjugate fidelity. In addition to waveguide area and the number of modes, which Hellwarth also included, the final

stages of this model include a rudimentary pump depletion weighting term, introducing a power dependence that is absent from Hellwarth's analysis. While the detailed analysis of the results is presented later, the model constructed here predicts that Hellwarth's analysis tends to severely underestimate the fiber length required. For example, while Equation (2.37) requires less than 2.22 meters of 0.06 NA fiber for $r_0 = 0.2$, the model predicts a 15 meter length of fiber is still adequate. This longer fiber will require a much lower pump power to cross SBS threshold, making device construction much easier and practical than it would initially appear from Hellwarth's inequality. These relaxed fiber length restrictions have been verified experimentally. In addition, another phenomenon, step index beam cleanup, is predicted, explained, and experimentally verified [21].

III. Modeling and Specific Theory

Foundations of the Model

The objective of this thesis was to generate theoretical predictions, based on a numerical model constructed in Matlab, of how the Stokes gain or backscattered power varies in a multimode fiber as one of many variables, including fiber length, input pump power, and number of excited modes, are varied. Specifically, this model was geared towards investigating the behavior of phase conjugate forms of the Stokes, and how these configurations compare to other arrangements, such as the fundamental mode or random modal distributions. The previous chapter started from basic principles and worked through to the critical term in this Stokes gain/power dependence, given in Equation (2.33). There are many terms in this expression, including amplitudes, phases, propagation constants, and transverse profiles, each of which changes depending on the mode being described. In addition, there are longitudinal change terms, $\kappa_{p,s}(z)$, which have been assumed, for simplicity, to be common to all modes. The amplitude and phase terms for the pump are user inputs, depending on what sort of pump is being considered. The amplitudes and phases of the Stokes beam are easily determined from the pump input if a phase conjugate beam is being considered. If not, then the Stokes configuration is again under the user's control. This leaves the longitudinal propagation constant, transverse profiles, and $\kappa_{p,s}(z)$ terms to quantify.

The propagation constants of the allowed modes can be found from the fiber's physical parameters, including core size and indices of refraction in the core and cladding. This is accomplished by using the fiber parameters to calculate its normal-

ized frequency, the V parameter. Noting that Equation (2.17) is a function only of V and k_T, the transverse propagation constant, a numerical root-finder was used to find all the allowed k_T values for a given V. The longitudinal propagation constant, β, is related to k_T by Equation (2.13). The algorithm was constructed such that two matrices were created, one each for β and k_T, where the row and column of each propagation constant indicated the $\ell + 1$ and m values, respectively. Forbidden modes were given entries of zero. Note that ℓ is not simply the row value itself because ℓ takes integer values beginning with zero, whereas Matlab indexes its arrays beginning with one.

For many multimode fibers, hundreds of modes are allowed, which would give prohibitively long computation times, so functionality was included in the model to input a given pair of arrays representing the k_T and β propagation constants, and only keep the values for a user input number of 'lowest' modes, N. Since the lower order longitudinal propagation constants have larger numerical values, this amounted to a simple numerical sorting routine. However, those modes with odd values of ℓ have a non-degenerate companion mode formed by a 90° rotation in the transverse plane which shares the same β value, and thus copies of these propagation constants must be created before the numerical sorting is performed so that these values are double counted. In addition, if the user inputs a certain number of modes, say $N = 10$, but the 10th mode actually has a rotated companion, then both modes will be included for completeness. The output of this algorithm was two matrices of a form similar to that described above, except higher order modes have been eliminated until the user input

37

value of modes was reached. Due to the ambiguity mentioned above, the number of modes actually included, counting rotated companion modes, was also output, where this value is either N or $N + 1$. It is worth noting that when the model is being used to compare to experimental results, using this routine to cut out the higher fiber modes could introduce significant error. Therefore, in the later results of the model that were intended to aid in experimental work, low NA fibers were used where the model could easily handle all the fiber modes.

With the transverse propagation constant it is possible to find the transverse electric field dependence, $\psi(r_\perp)$, which is formed from the product of the radial and azimuthal dependence described by Equations (2.10) and (2.16), and is normalized such that Equation (2.28) is satisfied. A grid of x and y values is created that covers the fiber core, where the number of gridpoints is a user input. A higher number of gridpoints gives finer detail in the transverse irradiance profiles, but requires longer computation times. For all the work presented in this thesis, a 40 x 40 pixel grid was used to depict the fiber core, which was more than adequate to capture the irradiance pattern detail while preserving reasonably short computation times. The product of Equations (2.10) and (2.16) is then taken at each grid point. As this is an irradiance profile, the imaginary exponential in the azimuthal dependence becomes a cosine. The output is a four dimensional array: the first two dimensions describe the x and y coordinates of the transverse intensity profile for the $LP_{\ell m}$ mode, ℓ is given by the third dimension coordinate minus one, and m is given by the fourth dimension.

Table 3.1. A summary of the three categories of solutions that are explored in this thesis. They are distinguished by the varying forms that the decay/growth of power in the pump/Stokes beams takes as one moves along the fiber.

	$\kappa_P(z)^2$	$\kappa_S(z)^2$
No pump depl.	1	N/A - separate var.
Decoupled no pump depl.	1	$e^{-g*I_{P0}*z}$
Pump depl.	$f(I_{P0})$	N/A - separate var.

With the amplitudes and phases, propagation constants, and transverse intensity profiles of each mode, the only pieces still missing from Equation (2.33) are the $\kappa_{p,s}(z)$ terms describing the longitudinal rate of change of the amplitudes. How these terms are handled forms the basis for the different categories of solutions, as summarized in Table (3.1).

While a detailed analysis of each solution is presented in the sections below, it is instructive to briefly review the rationale for why these three solutions were considered. If one plugs the pump and Stokes intensity product, Equation (2.33), into the lossless form of Equation (2.26b), one will see that to obtain a total backscattered Stokes power, an integration in the transverse plane and along z will have to be performed. Integrating in the transverse plane poses no difficulty, as this transverse dependence is isolated in the ψ_{ppss}^{ijnm} term. However, integrating along z poses a challenge. It has already been mentioned that a full solution to this problem would involve a coupled set of differential equations, which have caused serious difficulties for previous authors exploring SBS phase conjugation in free space [17]. To avoid this issue, we assumed a common longitudinal rate of change for all the modes, as written in Equation (2.32). To proceed further, one must still specify what form these
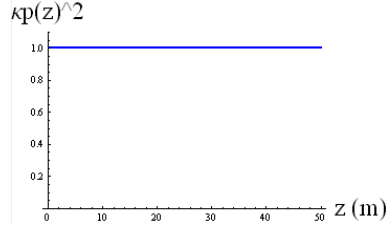
(a) $\kappa_P(z)^2$ in the no pump depletion solution.
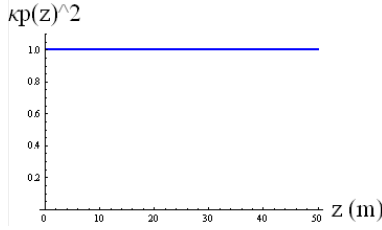
(b) $\kappa_P(z)^2$ in the decoupled no pump depletion solution.
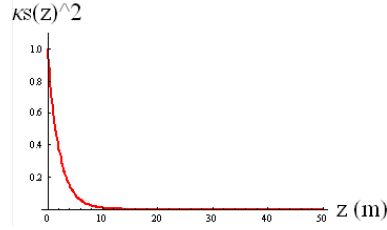
(c) Example of $\kappa_S(z)^2$ in the decoupled no pump depletion solution.
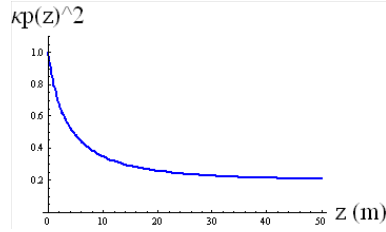
(d) Example of $\kappa_P(z)^2$ in the pump depletion solution.

Figure 3.1.   The $\kappa_{p,s}(z)^2$ weighting terms in the three different model solutions.

simplified versions of $\kappa_{p,s}(z)^2$ take. At first, simplicity was the goal, so $\kappa_p(z)^2 = 1$ was assumed, with $\kappa_s(z)^2$ not specified due to a separation of variables solution. In this solution, the pump experiences no loss throughout the fiber, as shown in Figure (1(a)). Obviously this is not true as, even in a lossless fiber, the power for the growing Stokes beam comes from the pump, which must be depleted to conserve energy. However, the resulting integration along z can now be done analytically, and even this simplified form makes some accurate predictions, as will be shown below.

The drawback to this initial solution was that all parts of the fiber are weighted equally. In reality, above SBS threshold the Stokes beam experiences the vast majority of its growth near the pump input end of the fiber. Since the Stokes irradiance is much larger at the front end of the fiber, it seemed logical to weight this end of the fiber more heavily. To this end, a simple exponential form for $\kappa_s(z)^2$ was introduced, with $\kappa_p(z)^2 = 1$ still holding true, as shown in Figures (1(b)) and (1(c)). Again, a closed form integration along z can be performed. It turns out that this exponential dependence gives too much weighting to the pump input end of the fiber. That is, the far end of the fiber contributes virtually nothing to the final result because $\kappa_s(z)^2 \approx 0$, an observation that is not born out experimentally [19, 21].

In an attempt to bridge the gap between these two extremes, a plane wave pump depletion approach was introduced. If we ignore the multimode nature of the fiber and treat it as single-mode, one can follow a standard derivation of how, for a given fiber and pump input power, the pump power will decay and the Stokes beam will grow throughout said fiber [14]. As can be seen in Figure (1(d)), the resulting $\kappa_P(z)^2$ does more heavily weight the front end of the fiber, but does not decay to zero at longer fiber lengths, allowing the solution to change as the fiber is lengthened. It will be seen that this solution comes the closest to matching the experimental data.

The No Pump Depletion Solution

The simplest approach is to ignore pump depletion altogether, such that $\kappa_p(z) = 1$, and treat the multimode fiber as lossless, such that $-\alpha_s I_s(r_\perp, z)$ in Equation (2.26b)

can be ignored. With these assumptions, one can plug Equation (2.33) into what remains of Equation (2.26b). Experimentally, the more easily observed quantities are usually powers, not irradiances, so one can integrate the resulting equation over the transverse spatial dimensions to give:

$$
\begin{aligned}
\frac{\partial P_s(z)}{\partial z} = &- g(\varepsilon_0 cn)^2 P_s(z) \times \\
&\frac{\sum_{f,q,j,\nu} A_{ppss}^{fqj\nu} \gamma_{ppss}^{fqj\nu} \cos(\Delta\beta_p^{fq} z + \Delta\phi_p^{fq}) \cos(\Delta\beta_s^{j\nu} z + \Delta\phi_s^{j\nu})}{P_s(0)}
\end{aligned}
\tag{3.1}
$$

where the substitution $\kappa_s(z)^2 = \frac{P_s(z)}{P_s(0)}$ has been made, and:

$$
\gamma_{ppss}^{fqj\nu} = \int \psi_{ppss}^{fqj\nu}(r_\perp)\, dr_\perp
\tag{3.2}
$$

describes the integrated product of four modal transverse electric field terms. One can now easily separate variables in Equation (3.1) by dividing through by $P_s(z)$ and multiplying by dz, which, after integrating both sides, eventually yields [16]:

$$
P_s(z) = P_s(0)e^{-G_{eff}(z)}
\tag{3.3}
$$

$$G_{eff}(z) = \frac{g(\varepsilon_0 cn)^2}{P_s(0)} \sum_{f,q,j,\nu} A_{ppss}^{fqj\nu} \gamma_{ppss}^{fqj\nu} \int_0^z \cos(\Delta\beta_p^{fq} z' + \Delta\phi_p^{fq}) \cos(\Delta\beta_s^{j\nu} z' + \Delta\phi_s^{j\nu}) \, dz'$$

$$= \frac{g(\varepsilon_0 cn)^2 z}{2 P_s(0)} \sum_{f,q,j,\nu} A_{ppss}^{fqj\nu} \gamma_{ppss}^{fqj\nu} \times$$

$$\left\{ \mathrm{sinc}\left[\frac{1}{2}(\Delta\beta_p^{fq} - \Delta\beta_s^{j\nu})z\right] \cos\left[\frac{1}{2}(\Delta\beta_p^{fq} - \Delta\beta_s^{j\nu})z + (\Delta\phi_p^{fq} - \Delta\phi_s^{j\nu})\right] \right.$$

$$+ \left. \mathrm{sinc}\left[\frac{1}{2}(\Delta\beta_p^{fq} + \Delta\beta_s^{j\nu})z\right] \cos\left[\frac{1}{2}(\Delta\beta_p^{fq} + \Delta\beta_s^{j\nu})z + (\Delta\phi_p^{fq} + \Delta\phi_s^{j\nu})\right] \right\} \quad (3.4)$$

It has already been discussed how one can determine the propagation constants that lead to $\Delta\beta_{p,s}$, as well as the transverse field profiles which give γ_{ppss}. The amplitude, A_{pp}, and phase, $\Delta\phi_p$, terms are user inputs while A_{ss} and $\Delta\phi_s$ are either user inputs or found by a Stokes gain maximization algorithm described later in this thesis. In either case, these latter amplitude and phase terms are not determined *a priori* by the physical characteristics of the fiber.

It is now relatively straightforward to use Equation (3.4) to compare the effective gain of the Stokes for various amplitude and phase configurations. Typically, a ratio of two different $G_{eff}(z)$ terms is taken so that the constants in front of the summation in Equation (3.4) cancel. The advantage of this no pump depletion approach is obvious simplicity. The longitudinal integration down the length of the fiber yields a closed form solution, and thus modeling of the gain for various fiber lengths can proceed very quickly. The downside is that this solution ignores pump depletion, and thus quickly loses validity as the SBS threshold is approached and exceeded.

The Decoupled No Pump Depletion Solution

A closed form solution has been described above that ignores pump depletion effects in the fiber, that is $\kappa_p(z)^2 = 1$. While straightforward, in developing this approach it was anticipated that it would lead to an underestimation of the phase conjugate fidelity that was attainable with a given fiber length. This is the same problem that has been encountered with previous models [8]. In an attempt to fix this problem, but maintain the simplicity found in an analytic solution, this section forces $\kappa_s(z)^2$ to take a decaying exponential form such that the pump input end of the fiber, where a good phase conjugate Stokes will have maximum overlap with the pump, is weighted much more heavily than the back end of the fiber. The physical rationale for this weighting is that the counterpropagating Stokes beam grows very rapidly in the final section of fiber near the pump input, and that the pump-Stokes overlap in this high power region should be more important than in the far end of the fiber, where the Stokes power is negligible. This weighting will artificially favor a phase conjugate, even at long fiber lengths.

If one again considers the no pump depletion case and ignores loss in the fiber, Equation (3.1) describing the longitudinal rate of change of the Stokes power can be rewritten, though this time $\kappa_s(z)^2 \neq \frac{P_s(z)}{P_s(0)}$, leaving:

$$\frac{\partial P_s(z)}{\partial z} = -g(\varepsilon_0 cn)^2 \sum_{f,q,j,\nu} A_{ppss}^{fqj\nu} \gamma_{ppss}^{fqj\nu} \kappa_s(z)^2 \cos(\Delta\beta_p^{fq} z + \Delta\phi_p^{fq}) \cos(\Delta\beta_s^{j\nu} z + \Delta\phi_s^{j\nu})$$

$$(3.5)$$

In the previous section, the $\kappa_s(z)^2$ was eliminated at the cost of introducing a $\frac{P_s(z)}{P_s(0)}$ term, but it was easy to perform a separation of variables leading to a solution for the gain of the Stokes. Now, $\kappa_s(z)^2$ will be forced to take a certain form on the right side of Equation (3.5), while solving for $P_s(z)$ on the left side. Thus, the Stokes z dependence is specified on the right side, while it takes a different, unknown form on the left side. This is what is meant by a 'decoupled' no pump depletion solution.

A simple weighting factor can be obtained by solving Equation (2.26b) in a lossless singlemode fiber where we assume the mode uniformly fills the entire core, and the pump is not depleted, giving the starting equation:

$$\frac{\partial I_s(z)}{\partial z} = -gI_p(0)I_s(z) \tag{3.6}$$

which can easily be solved by separation of variables to give:

$$\frac{I_s(z)}{I_s(0)} = \kappa_s(z)^2 = e^{-gI_p(0)z} \tag{3.7}$$

One can plug this plane wave expression for $\kappa_s(z)^2$ into Equation (3.5) and integrate along the fiber to yield:

$$P_s(z) - P_s(0) = -g(\varepsilon_0 cn)^2 \sum_{f,q,j,\nu} A_{ppss}^{fqj\nu} \gamma_{ppss}^{fqj\nu} \times$$
$$\int_0^z e^{-gI_p(0)z'} \cos(\Delta\beta_p^{fq} z' + \Delta\phi_p^{fq}) \cos(\Delta\beta_s^{j\nu} z' + \Delta\phi_s^{j\nu}) \, dz' \tag{3.8a}$$

45

$$P_s(0) = P_s(z) + g(\varepsilon_0 cn)^2 \sum_{f,q,j,\nu} A_{ppss}^{fqj\nu} \gamma_{ppss}^{fqj\nu} \left\{ \frac{e^{-\xi z}}{2} \times \right.$$

$$\left[\frac{k_-^{fqj\nu} \sin(k_-^{fqj\nu} z + \phi_-^{fqj\nu}) - \xi \cos(k_-^{fqj\nu} z + \phi_-^{fqj\nu})}{\xi^2 + (k_-^{fqj\nu})^2} + \right.$$

$$\left. \frac{k_+^{fqj\nu} \sin(k_+^{fqj\nu} z + \phi_+^{fqj\nu}) - \xi \cos(k_+^{fqj\nu} z + \phi_+^{fqj\nu})}{\xi^2 + (k_+^{fqj\nu})^2} \right] -$$

$$\left. \frac{1}{2} \left[\frac{k_-^{fqj\nu} \sin(\phi_-^{fqj\nu}) - \xi \cos(\phi_-^{fqj\nu})}{\xi^2 + (k_-^{fqj\nu})^2} + \frac{k_+^{fqj\nu} \sin(\phi_+^{fqj\nu}) - \xi \cos(\phi_+^{fqj\nu})}{\xi^2 + (k_+^{fqj\nu})^2} \right] \right\} \qquad (3.8b)$$

where several terms have been introduced to simplify Equation (3.8b):

$$\xi = gI_p(0) \qquad (3.9a)$$

$$k_\pm^{fqj\nu} = \Delta k_p^{fq} \pm \Delta k_s^{j\nu} \qquad (3.9b)$$

$$\phi_\pm^{fqj\nu} = \Delta \phi_p^{fq} \pm \Delta \phi_s^{j\nu} \qquad (3.9c)$$

For input pump powers above the SBS threshold, the $P_s(z)$ term on the right side in Equation (3.8b) is negligible compared to $P_s(0)$ and can be dropped. It is also noted that, because a separation of variables was not performed, Equation (3.8b) gives the backscattered Stokes power, not an effective gain like Equation (3.4), though the power and gain are obviously related.

Previously in Equation (3.4), the z dependence was found only in trigonometric terms, including a *sinc*, that could remain appreciable at large z values if $\Delta \beta_p^{fq} \pm \Delta \beta_s^{j\nu}$ was small. Thus, making the fiber arbitrarily long had consequences for the final result. Now, Equation (3.8b) contains a power dependence in the $e^{-\xi z}$ decaying ex-

ponential term that is absent in Equation (3.4). This exponential has no modal dependence, and will greatly decrease the importance of all the z dependent trigonometric terms in the summation as z is increased. Thus, it is expected that solutions obtained with this equation will taper off to a constant value for large fiber lengths, where this constant is found from the z independent terms in Equation (3.8b).

The Pump Depletion Solution

The previous section introduced a rudimentary power dependence by forcing the Stokes to grow exponentially in the counterpropagating direction, while the pump remained constant throughout. There are two main problems with this approach that counter its simplicity. First, while for low pump input powers that are well below SBS threshold this no pump depletion approximation is a good one, these conditions are of little interest in modeling a practical SBS phase conjugate mirror, as there will be almost no backscattered power far below SBS threshold. As the pump power is increased, the backscattered Stokes power will increase, especially at the pump input end of the fiber. To conserve energy, the pump power must be depleted as it propagates through the fiber, that is $\kappa_p(z)^2 \neq 1$. Neither of the above solutions includes this physical aspect of the problem.

Secondly, the exponential dependence of $\kappa_s(z)^2$ in the decoupled solution will strongly weight the pump input end of the fiber above SBS threshold, virtually ignoring the impact of the majority of the fiber's length. This would imply that high quality phase conjugation is possible in an arbitrarily long fiber length, as long as the

47

pump input power is above SBS threshold, a conclusion that is not supported by the majority of the experimental evidence [19, 21]. As will be shown below, it is more mathematically rigorous to not assume an expression for $\kappa_s(z)^2$, but rather introduce a pump depletion term, such that $\kappa_p(z)^2 \neq 1$.

If one again starts with Equation (3.1), except now including pump depletion, one obtains:

$$
\frac{\partial P_s(z)}{\partial z} =
$$
$$
- \eta P_s(z) \frac{\sum_{f,q,j,\nu} A_{ppss}^{fqj\nu} \gamma_{ppss}^{fqj\nu} \kappa_p(z)^2 \cos(\Delta\beta_p^{fq} z + \Delta\phi_p^{fq}) \cos(\Delta\beta_s^{j\nu} z + \Delta\phi_s^{j\nu})}{P_s(0)} \quad (3.10)
$$

where $\eta = g(\varepsilon_0 c n)^2$. By dividing through by $P_s(z)$ and integrating both sides over z, one finds:

$$
P_s(z) = exp \left[-\eta \frac{\sum_{f,q,j,\nu} A_{ppss}^{fqj\nu} \gamma_{ppss}^{fqj\nu} \int_0^z \kappa_p(z')^2 \cos(\Delta\beta_p^{fq} z' + \Delta\phi_p^{fq}) \cos(\Delta\beta_s^{j\nu} z' + \Delta\phi_s^{j\nu}) dz'}{P_s(0)} \right]
$$
$$
(3.11)
$$

To proceed further, an expression for $\kappa_p(z)^2$ is required.

A logical starting point in estimating this new form of $\kappa_p(z)^2$ is to again look at a lossless, singlemode fiber whose core is uniformly filled by the mode, the same assumption made above in writing Equation (3.6), except now we look at the depleted pump case. In this situation, Equations (2.26a) and (2.26b) can be written:

$$
\frac{\partial I_{s,p}(z)}{\partial z} = -g I_p(z) I_s(z) \quad (3.12)
$$

48

where the $r_\perp$ dependence is not required in a singlemode fiber, and the ω_p/ω_s term in Equation (2.26a) is very close to one with SBS. The two equations represented by (3.12) imply that $I_p(z) = I_s(z) + C$, where C is a integration constant. This allows one to re-write the differential equation in terms of just the Stokes intensity, and after a separation of variables one finds that the Stokes intensity is given by [14]:

$$I_s(z) = \frac{I_s(0)[I_p(0) - I_s(0)]}{I_p(0) \exp\{gz[I_p(0) - I_s(0)]\} - I_s(0)} \tag{3.13}$$

The pump takes a similar form because $I_p(z) = I_s(z) + C = I_s(z) + I_p(0) - I_s(0)$. After dividing through by $I_p(0)$, one finds that:

$$\kappa_p^2(z) = \frac{I_s(0)[I_p(0) - I_s(0)]}{I_p^2(0) \exp\{[gz[I_p(0) - I_s(0)]\} - I_s(0)I_p(0)} + 1 - \frac{I_s(0)}{I_p(0)} \tag{3.14}$$

The problem with this form of the longitudinal intensity dependence is that it is in terms of $I_p(0)$ and $I_s(0)$ when, in the conditions of interest here, only $I_p(0)$ is under one's direct control in the lab.

SBS originates in spontaneous Brillouin scattering at the far end of the fiber where $z = L$, opposite the pump input. This spontaneous scattering is linear with respect to the pump intensity, so that one can write:

$$I_s(L) = fI_p(L) \tag{3.15}$$

If we consider $z = L$ then Equation (3.13) can be written as:

$$\frac{I_s(L)}{I_p(0)} = \frac{R(1-R)}{\exp[G(1-R)] - R} \tag{3.16}$$

where $R \equiv I_s(0)/I_p(0)$ represents the SBS reflectivity, and $G = gI_p(0)L$ gives the theoretical SBS gain along the full length of the fiber with an undepleted pump. The $I_s(L)$ on the left side of Equation (3.16) is not an easily observed quantity, and would ideally be eliminated from the final result. Using the fact that $I_s(z)$ and $I_p(z)$ differ only by a constant, one can write:

$$I_p(L) - I_s(L) = I_p(0) - I_s(0) \tag{3.17}$$

Since f in Equation (3.15) is typically very small, on the order of 10^{-12} to 10^{-11}, the $I_s(L)$ term on the left side of Equation (3.17) can be neglected. By writing $I_p(L)$ as $I_s(L)/f$ and rearranging terms, one finds that $I_s(L)/I_p(0) = f(1-R)$. Substituting this result into Equation (3.16) one finds:

$$\frac{G}{G_{th}} = \frac{G_{th}^{-1} \ln R + 1}{1-R} \tag{3.18}$$

where $G_{th} = -\ln f$ [14]. If one knows the input pump power and fiber length, one can calculate G. G_{th} typically takes a value of approximately $20-30$ in most fibers, though it can easily be determined for a specific fiber by experimentally observing that fiber's SBS threshold and then adjusting G_{th} until Equation (3.18) gives an appreciable R.

With G and G_{th} determined in this way, it is trivial to solve transcendentally for R, which gives $I_s(0)$ since one already knows $I_p(0)$. This value of $I_s(0)$ can then be used in Equation (3.14) to give the z dependence of the pump along the fiber, which then allows one to solve for the exponential gain term of the Stokes in Equation (3.11). Unlike the two no pump depletion solutions given above, the integral in Equation (3.11) does not have an analytic solution and is evaluated numerically in the model. This numerical integration can take a prohibitively long time if all of the modal permutations in the quadruple summation are included.

Thankfully, to a very good approximation, many of the terms can be thrown out in a manner similar to that employed in Hellwarth's perturbation treatment [8]. If one uses the product to sum trigonometric identities, one can express the cosines in Equation (3.11) by:

$$
\cos(\Delta\beta_p^{fq} z + \Delta\phi_p^{fq}) \cos(\Delta\beta_s^{j\nu} z + \Delta\phi_s^{j\nu}) =
$$
$$
\frac{1}{2} \left\{ \cos[(\Delta\beta_p^{fq} - \Delta\beta_s^{j\nu})z + \Delta\phi_p^{fq} - \Delta\phi_s^{j\nu}] + \cos[(\Delta\beta_p^{fq} + \Delta\beta_s^{j\nu})z + \Delta\phi_p^{fq} + \Delta\phi_s^{j\nu}] \right\}
$$
$$
(3.19)
$$

Consider a typical multimode silica fiber with a numerical aperture of 0.14 at a wavelength of 1064 nm, and core radius of $20\mu m$. Such a fiber supports approximately 55 LP modes of a single polarization. Looking at all the modal permutations that give rise to the $\Delta\beta_p^{fq}$ terms, the magnitude of the smallest nonzero $\Delta\beta_p^{fq}$ is approximately 71 m^{-1}. This case is exceptionally low, and most of the terms are much higher, into

the thousands of inverse meters. The large magnitude of these $\Delta\beta$ terms implies that, unless there is a special relationship between f, q, j and ν, $(\Delta\beta_p^{fq} \pm \Delta\beta_s^{j\nu})z$ will oscillate very rapidly as one moves z along the fiber, and integrate to nearly zero. These special cases are explored below.

When $f = q$ and $j = \nu$ the arguments of the cosines go to zero, meaning the cosines go to one and the integral along the fiber degenerates to an integral of $\kappa_p^2(z)$. The $\Delta\beta$ terms can also go to zero even when $f \neq q$ and $j \neq \nu$ because distinct modes that are related by a 90° rotation in the transverse plane share a common propagation constant, though the starting phases will generally not be the same. However, these terms generally make a negligible contribution to the overall result, and are thus left out of the model, due to the $\gamma_{ppss}^{fqj\nu}$ term. By rotating these modes 90° and taking the product, the maxima of one mode will multiply the minima of its counterpart, leading to a much smaller result, on average, when the integration in the transverse plane is taken [8].

For the final special permutation of propagation constants, consider only the $\cos[(\Delta\beta_p^{fq} - \Delta\beta_s^{j\nu})z + \Delta\phi_p^{fq} - \Delta\phi_s^{j\nu}]$ beat frequency. Isolating one specific difference of propagation constants $\Delta\beta_p^{ab}$, where $f = a$ and $q = b$ in the multimode fiber described above, one can numerically evaluate all the possible permutations of $\Delta\beta_p^{fq}$ and show that the closest value to $\Delta\beta_p^{ab}$ is still several hundred inverse meters off. That is, the chances of the difference between two propagation constants happening to be nearly equal to the difference of two other propagation constants are virtually zero, so we need only consider the situation where the two different pump modes match

the Stokes modes. Due to the very small wavelength shift of the Stokes relative to the pump, the propagation constants of these two wavelengths are nearly equal, revealing that $\Delta\beta_p^{fq} - \Delta\beta_s^{fq}$ yields a small result, typically a fraction of an inverse meter. This gives a cosine that varies slowly enough that it will lead to a non-zero result from the integration in Equation (3.11).

This same argument can be applied to the $\cos[(\Delta\beta_p^{fq} + \Delta\beta_s^{j\nu})z + \Delta\phi_p^{fq} + \Delta\phi_s^{j\nu}]$ term, except the ordering of the indices of the pump propagation constants relative to the Stokes are reversed. That is, the above sum frequency cosine term will vary slowly when $f = \nu$ and $q = j$ so that $\Delta\beta_p^{fq} + \Delta\beta_s^{qf} = \Delta\beta_p^{fq} - \Delta\beta_s^{fq}$ which can again be less than an inverse meter.

Thus, summarizing the above arguments, the remaining analysis assumes:

$$\cos(\Delta\beta_p^{fq}z + \Delta\phi_p^{fq})\cos(\Delta\beta_s^{j\nu}z + \Delta\phi_s^{j\nu})$$

$$\simeq \begin{cases} \frac{1}{2}\cos[(\Delta\beta_p^{fq} - \Delta\beta_s^{j\nu})z + \Delta\phi_p^{fq} - \Delta\phi_s^{j\nu}] & \text{, if } f = j \text{ and } q = \nu \neq f \\ \frac{1}{2}\cos[(\Delta\beta_p^{fq} + \Delta\beta_s^{j\nu})z + \Delta\phi_p^{fq} + \Delta\phi_s^{j\nu}] & \text{, if } f = \nu \text{ and } q = j \neq f \\ 1 & \text{, if } f = q \text{ and } j = \nu \\ 0 & \text{, otherwise} \end{cases} \tag{3.20}$$

Plugging Equations (3.20) and (3.14) into (3.11) gives the backscattered Stokes power, within the limit of the approximations mentioned above.

IV. Results and Analysis

The No Pump Depletion Solution

The no pump depletion model can be used to calculate the effective gain, G_{eff}, that was described in Equation (3.4). Remember that this solution ignores depletion of the pump power, and thus gives equal weighting to what is happening at the far end of the fiber as to what occurs at the pump input end. The absolute value of G_{eff} would be hard to interpret, and so all the results presented below are ratios of G_{eff} for one form of the Stokes to another, thus all the terms in front of the summation in Equation (3.4) cancel. A result greater than one indicates that the backscattered Stokes would resemble the modal configuration in the numerator, given the two options represented by numerator and denominator.

The notation zPC is used throughout this thesis to indicate which phase conjugate is being discussed, specifically, where along the fiber the Stokes irradiance pattern matches that of the pump. To the experimentalist, a perfect phase conjugate would have a $zPC = 0$ m, because the backscattered Stokes would match the pump as the fiber ends and the pattern can be observed in free space with a camera. This is the meaning of phase conjugate that is assumed in most of the literature. As another example, a $zPC = 50$ m would indicate that, if one could observe the irradiance pattern inside the fiber, the Stokes would match the pump 50 meters down the fiber relative to the pump input. Due to the small redshift of the Stokes relative to the pump, this Stokes will not match the pump at $z = 0$ m. The unspecified term 'phase conjugate' refers to the traditional $zPC = 0$ m case, while other phase conjugate forms will al-
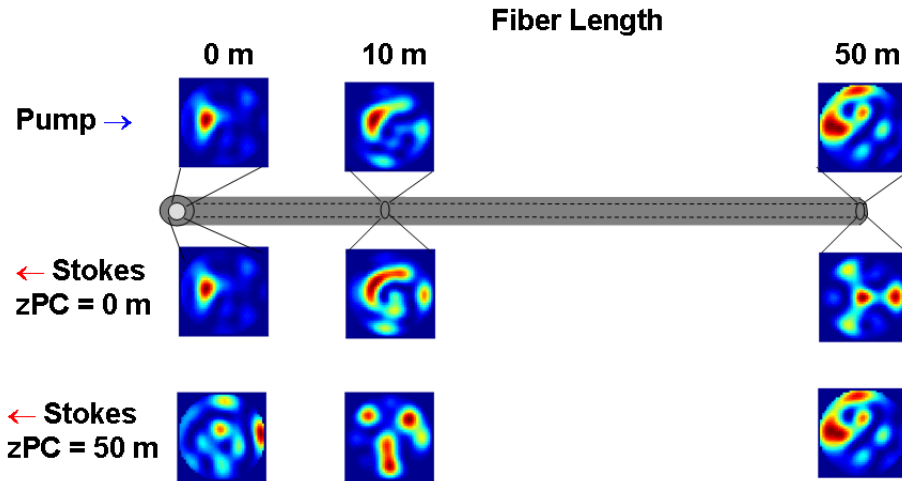
Figure 4.1.   Sample irradiance patterns at different points within the fiber for Stokes beams with different zPC values.

ways be specified with their zPC value. For any zPC value, the amplitudes of a given mode match in the pump and Stokes beam, that is $A_p^i = A_s^i$ for mode i. Changing zPC just varies the modal phases.

Figure (4.1) clarifies this concept. A multimode pump beam is shown at the top, which evolves, due to the varying propagation constants for each mode, such that the irradiance pattern varies as one moves along the fiber. Two sample backscattered Stokes beams are shown below the fiber. The first is the 'perfect' phase conjugate, with $zPC = 0$ m, such that the pump and Stokes irradiance patterns match at the pump input end of the fiber. Due to the small wavelength shift between pump and Stokes, as one moves through the fiber the Stokes irradiance pattern diverges from the pump, such that at 10 m a small discrepancy is apparent, and at 50 m there is little or no resemblance to the pump. For the $zPC = 50$ m Stokes beam, at the front

end of the fiber the Stokes bears no relation to the pump, but as one moves through the fiber to $z = 50$ m, the Stokes begins to more closely resemble the pump, and at 50 m they exactly match. All three beams have the same amplitudes for each mode, it is only the phases that differ from one beam to the other.

Beam cleanup is an effect whereby a multimode pump input yields a single mode backscattered Stokes output. In graded index fibers, where the index of refraction varies continuously in the core, beam cleanup to the fundamental mode is observed in long fibers, while phase conjugate outputs may be seen with shorter fibers. For the step index fibers that are the focus of this thesis, phase conjugation is still obtained for short fibers, but beam cleanup is generally not observed as the length is increased, except under very special launching conditions. The discussion of this specialized case of beam cleanup will be deferred to the end of the chapter. The ratio of the effective gain of the 'traditional' $zPC = 0$ m phase conjugate form of the Stokes to a Stokes beam in the fundamental mode was taken to see how these two special Stokes beams compare to one another.

The plot shown in Figure (4.2) clearly indicates that for short fibers the phase conjugate has a higher gain than the fundamental mode, but as the fiber length is increased this advantage quickly decreases. For fibers longer than 20 meters the phase conjugate has a gain roughly equal to that of the fundamental mode, and thus loses its advantage in dominating the output. In Lombard's work, it was observed that in short step index fibers, good phase conjugation was obtained, while in longer step index fibers, neither phase conjugation nor cleanup to the LP_{01} fundamental

56
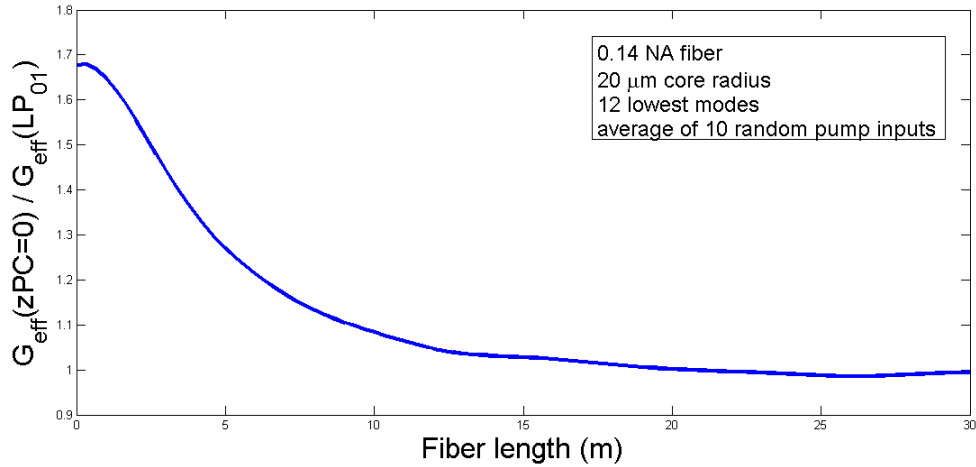
Figure 4.2.   Comparison of the ratio of phase conjugate to fundamental mode effective gains in the no pump depletion approximation as a function of fiber length

mode was seen [19]. While the fiber modeled here does not match the one used in Lombard's work, the model still correctly predicts the qualitative trend that the phase conjugate is favored in shorter fibers, and the difference in gain between these two Stokes outputs averages out as the fiber lengthens, with no clear preference. However, there is nothing special about the fundamental mode, which begs the question, how does the phase conjugate Stokes compare to other Stokes arrangements besides a perfect fundamental mode?

One can compare the $zPC = 0$ m Stokes gain to that of nonzero zPC values, as shown in Figure (4.3). Specifically, the effective gain for $zPC = 1.5$ m or 3 m was compared to $zPC = 0$ m for various fiber lengths. This was done for both the 12 and 24 lowest modes to simultaneously observe what effect, if any, higher order modes have on the results.
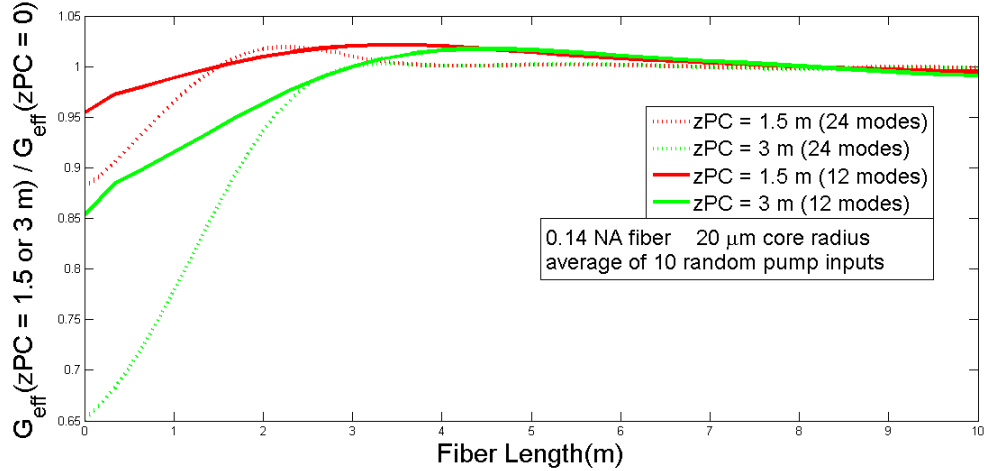
Figure 4.3.   Comparison of effective gains for various forms of the Stokes phase conjugate in the no pump depletion approximation. zPC represents the point along the fiber where the pump and Stokes would have matching intensity patterns. All results are normalized to the gain of the $zPC = 0$ m Stokes beam at the given fiber length.

The results for the 12 lowest modes indicate that for very short lengths, $zPC = 1.5$ m has a greater gain than $zPC = 3$ m, but both fall short of $zPC = 0$ m because the ratio is less than one. This is not surprising. For very short fibers, the $zPC = 0$ m Stokes will almost exactly match the pump throughout the fiber, and give a high gain. It should be noted that when the value for zPC is greater than the fiber length, the Stokes phases are chosen such that the pump and Stokes fields would match if the fiber were long enough.

As zPC is increased, the Stokes irradiance pattern will diverge from the pump at the input end of the fiber, decreasing the gain, which explains why $zPC = 3$ m has the lowest ratio for short fibers. As the fibers are lengthened, the $zPC = 0$ m Stokes gain grows more slowly than that for the other Stokes configurations because these latter forms of the Stokes more closely match the pump at these longer lengths of

58

$1 - 3$ meters. Eventually, the ratio of effective gains for both phase conjugate forms grows to slightly more than one. However, as the fiber is lengthened even more, both ratios quickly approach one, indicating that there is no clear advantage of one phase conjugate form over the other. Each point along the fiber is weighted equally and, as the fiber is lengthened, differences amongst various modal arrangements average out.

The results for the 24 lowest modes follow a similar pattern, with two principle differences. The initial performance of both the $zPC = 1.5$ and 3 m configurations relative to $zPC = 0$ m is worse, and the peak performance and subsequent averaging to near one occurs at shorter fiber lengths than was seen for the 12 lowest modes. The more modes one includes, the more rapidly the multimode irradiance pattern changes along the fiber. This implies that, as the number of modes is increased for a given nonzero zPC, the corresponding intensity pattern will diverge more rapidly from that of the pump at the $z = 0$ m end of the fiber. This leads to a lower ratio of effective gains for short fibers. This same rapid evolution of the intensity also means that differences among various starting Stokes arrangements will average out more quickly as the fiber is lengthened, leading to ratios of approximately one for shorter fibers than for the 12 mode case.

Comparisons of the traditional phase conjugate to the fundamental mode and to phase conjugates at a nonzero distance into the fiber have now been made with similar results. For very short fibers, the traditional phase conjugate has the highest gain, but as the fiber is lengthened the effective gains of all the possibilities approach the same value. The examples presented above are representative, but somewhat

Table 4.1.   Statistics on backscattered Stokes gains, normalized to the phase conjugate, obtained with the no pump depletion solution for 1000 random Stokes configurations relative to a single input pump.

fiber length	mean	max	min	std dev
1 m	0.521	0.7493	0.4368	0.0434
10 m	0.7562	0.9342	0.6483	0.0426
100 m	0.8534	0.8823	0.7384	0.0446

contrived. There are an infinite number of permutations of modal amplitudes and phases one can adjust, obviously not all of them can be explored.

To give a balance between practicality and investigating less contrived Stokes arrangements, the effective gain for multiple random Stokes patterns was calculated for a given pump input, and compared to the gain of the phase conjugate. For a 0.14 NA fiber of varying length, with a core radius of 20 μm, and considering only the 12 lowest modes, a single random pump input was created and the gain of the perfect phase conjugate at $zPC = 0$ m was calculated. A thousand random Stokes configurations were then generated, that is a thousand different sets of randomly chosen normalized amplitudes, A_s^j, and phase terms, ϕ_s^j. The effective gain was calculated for each random arrangement and normalized to the single gain of the $zPC = 0$ m Stokes found previously. The same set of random Stokes beams was used for each fiber length, with the results listed in Table (4.1).

It is clear that, as the fiber is lengthened, the mean normalized gain approaches unity, implying that an arbitrary combination of phases and normalized amplitudes will perform nearly as well as the phase conjugate. This is due to the same averaging effect previously mentioned. If equal importance is given to each point along a fiber

that is getting longer, then the differences between different Stokes patterns quickly average out.

Having considered the effective gain, described in Equation (3.4), of a variety of Stokes beams, several conclusions can be drawn. First, despite the many approximations made in this solution, Equation (3.4) still correctly predicts that beam cleanup to the fundamental LP_{01} mode will not dominate the Stokes output, even in long fibers. This is due to the second observed result, that the gains of all the possible Stokes configurations approach the same value as the fiber length is increased, as shown in Table (4.1), such that the backscattered Stokes would increasingly appear to have little relation to the pump input.

The Decoupled No Pump Depletion Solution

The previous section weighted all the points along the fiber's length equally, leading to the averaging effects discussed above. By forcing the Stokes to grow in the backscattered direction, while assuming the pump remains constant throughout the fiber, one can derive an equation for the backscattered Stokes power, shown in Equation (3.8b). Forcing the backscattered Stokes to grow while ignoring depletion in the pump is obviously a significant simplification. However, it has the major advantage of introducing some weighting to the pump input end of the fiber, yet retaining simplicity in the form of an integration along the fiber that yields a closed form result. This weighting introduces a new variable to investigate, the input pump power. To investigate the effect of this power dependence, the same three analyses

61

considered for the unweighted no pump depletion solution above will be repeated, now in the context of Equation (3.8b).

Again consider the comparison of the phase conjugate to fundamental Stokes. Previously, it was found that the phase conjugate enjoyed a higher effective gain for shorter fibers, though this difference decreased as the fiber was lengthened until the ratio of the two gains approached unity. Figure (4.4) shows a similar analysis except now two different pump powers are shown. Note that, due to the methods employed in its derivation, Equation (3.8b) gives the backscattered Stokes power, not an effective gain.

A low and high pump input of 0.1 and 5 W were both considered for the fiber analyzed in Figure (4.2). The low input power shows similar behavior to that of the unweighted NPD solution above, the phase conjugate enjoying a clear advantage for short fibers that quickly decreases to approximately one for longer fiber lengths. The higher input power of 5 W shows a similar trend, with the maximum ratio of phase conjugate to fundamental gain at the shortest fiber lengths. This maximum ratio matches the low power result because, for very short fibers, the SBS threshold is larger than the powers considered here, and so both powers degenerate to the same below threshold, equal weighting regime.

As the fiber is lengthened, the SBS threshold decreases and the weighting effects of the 5 W pump input are clearly seen. The front end of the fiber becomes more heavily weighted than the end opposite the pump. The irradiance pattern of the phase
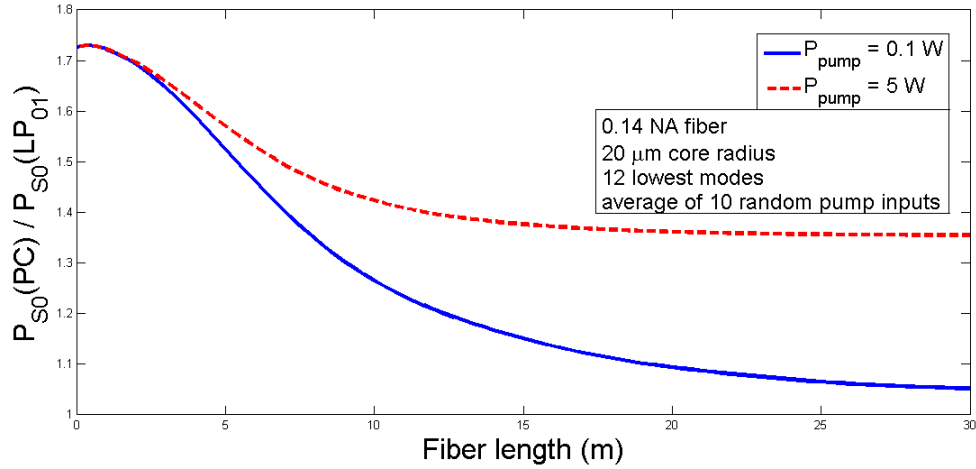
Figure 4.4.   Comparison of the ratio of phase conjugate to fundamental mode effective gains, in the decoupled no pump depletion approximation, as a function of fiber length

conjugate Stokes closely matches the pump at the front end of the fiber, leading to a higher product of these two intensities in Equation (2.26b). Weighting the fiber where the phase conjugate enjoys this advantage increases its backscattered power relative to other Stokes patterns. This is observed at the longer fiber lengths in Figure (4.4), where the high power result trails off to a Stokes power that is still approximately 1.35 times that of the fundamental mode. Thus, the phase conjugate now enjoys a performance advantage even at longer fiber lengths, where previously all Stokes patterns degenerated to a similar performance.

Analysis of the performance of one phase conjugate form to another was also repeated in Figure (4.5), which is very similar to Figure (4.3), except now the analysis is limited to the $zPC = 3$ m, 12 mode case, with the input pump power, P_{P0}, being varied. All results are again normalized to the $zPC = 0$ phase conjugate Stokes. Again, remember that the results are now ratios of backscattered Stokes powers, not
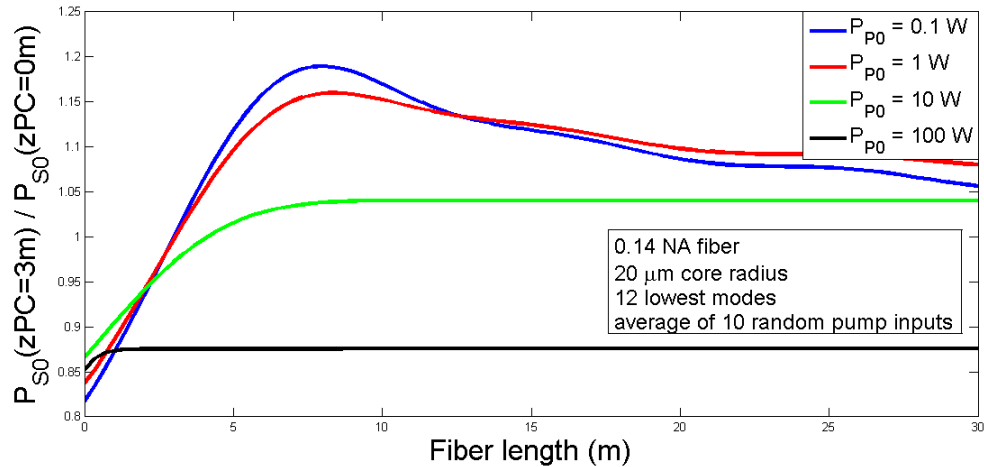
Figure 4.5.   Comparison of effective gains for various forms of the Stokes phase conjugate in the weighted no pump depletion approximation. zPC represents the point along the fiber where the pump and Stokes would have matching intensity patterns.

effective gains. For very short fibers, the results for all the input pump powers are comparable, which is not surprising because for these very short fibers there is not much space for a Stokes beam to grow.

As the fiber lengthens, all of the normalized powers increase, though as the pump power is lowered, the $zPC = 3$ m Stokes power increases relative to $zPC = 0$ m. This is again because the product of the Stokes and pump irradiance patterns for the $zPC = 3$ m case reaches a maximum 3 m into the fiber. For very low pump powers, the 3 m point is weighed nearly equal to the front end of the fiber, but as the pump is increased, the importance of this area of the fiber is lessened by the weighting factor in Equation (3.7) in favor of the pump input end of the fiber. This causes the decrease in the maximum of each curve, shown in Figure (4.5), as the pump power is increased. For very high pump powers, this ratio is always less than one, implying

64

that the $zPC = 3$ m Stokes beam always performs worse than the phase conjugate at the front of the fiber. For longer fibers, a very low pump power of 0.1 W gives a ratio that approaches one, similar to the unweighted case shown in Figure (4.3), due to the same averaging effects that are still present here, when well below SBS threshold. For long fibers with high pump powers, the ratio quickly approaches a constant value because the back end of the fiber has a negligible effect on the final result.

The model was also used to evaluate the gain of numerous random Stokes configurations, again normalized to the performance of the $zPC = 0$ Stokes, the results of which are seen in Table (4.2) and Figure (4.6), which are analogous to the data presented in the unweighted no pump depletion section except for the new power dependence. Six trials were considered: 1, 10, and 100 meter fibers, each of which was analyzed for an input pump power of 0.1 and 10 W. All trials were subjected to 1000 random Stokes inputs. The same pump input and set of 1000 possible random Stokes configurations were used for all of the analysis presented below, though a different 1000 arrangements were used for the analysis previously presented in Table (4.1).

Table 4.2.   Statistics on backscattered Stokes powers, normalized to the phase conjugate, obtained with the weighted no pump depletion method for 1000 random Stokes configurations relative to a single input pump.

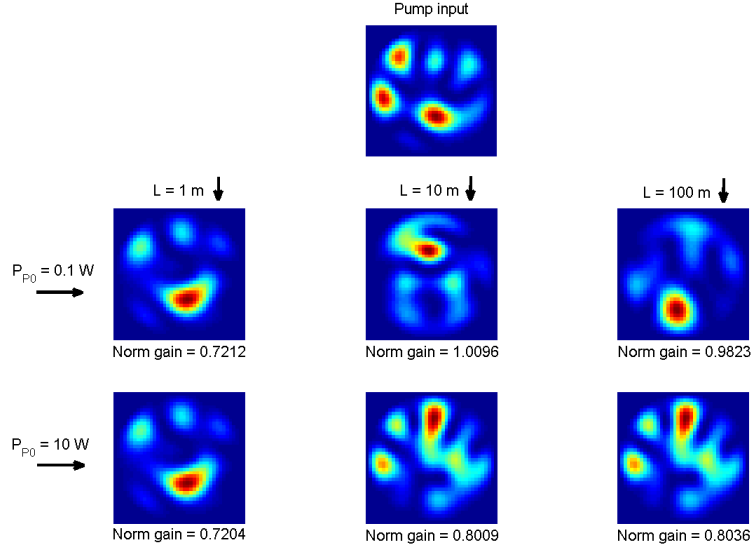| fib. length	P_{P0}	mean	max	min	std dev
1 m	0.1 W	0.5512	0.7219	0.4809	0.0409
10 m	0.1 W	0.7773	1.0096	0.6779	0.045
100 m	0.1 W	0.8891	0.9823	0.7899	0.0317
1 m	10 W	0.5508	0.7204	0.4806	0.0409
10 m	10 W	0.6286	0.8009	0.5517	0.0404
100 m	10 W	0.6332	0.8036	0.5565	0.0401

Figure 4.6.   The intensity patterns of an incident pump and the three Stokes beams that experienced maximum gain from 1000 random Stokes configurations. The 12 lowest modes in a 0.14 NA, $20\mu m$ radius core fiber were considered. A perfect Stokes phase conjugate would exactly match the pump input.

Multiple insights can be drawn from this data. First, the data for $P_{P0} = 0.1$ W is very similar to that presented in Table (4.1) for the unweighted no pump depletion approximation. This is not surprising, because an input pump power of only 0.1 W is very low and will not be sufficient to excite a Stokes wave in any of the fiber lengths, implying a relatively uniform weighting will occur. For a 10 W pump power, the statistical results for the 1 m fiber are very similar to those of the lower power case, again because 10 W is not high enough to excite a significant Stokes wave in so short a fiber. However, for the two longer fibers there are clear differences between high and low pump powers. All of the results, except for the standard deviation, drop in the high power case. This is to be expected because these results originally rose, as discussed in relation to Table (4.1), because of averaging effects in the longer fibers
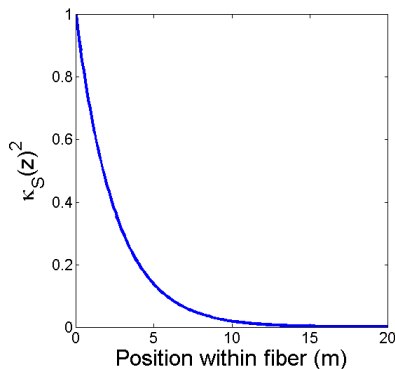
66

Figure 4.7.   Stokes weighting term as a function of distance along the fiber. Note exponential decrease to nearly zero.

which are now eliminated. Furthermore, there is very little difference between the 10 and 100 m fibers, and these fibers also share the same maximum performing Stokes beam, as shown in Figure (4.6).

The reason for the similarities between the 10 and 100 m fibers is obvious by plotting the $\kappa_s(z)^2$ used in this class of solutions, given in Equation (3.7), for 10 W of pump input power. The result is seen in Figure (4.7), where only the first 20 meters along the fiber are shown. It is obvious that the weighting term, $\kappa_s(z)^2$, declines to a very small value around the 10 m point, and thus lengthening the fiber past this point has little effect on the final results. In addition, $\kappa_s(z)^2 \approx 0.7$ at 1 m, which is indicative of the small effect weighting has on such a short fiber. In this class of solutions, $\kappa_s(z)^2$ is a simple decaying exponential and thus, for a long enough fiber, can become arbitrarily close to zero. Taking pump depletion into account will change this behavior such that, while the end of the fiber opposite the pump input is weighted less heavily than the front end, the weighting does not approach zero.

67

The Pump Depletion Solution

As mentioned above, while the exponential $\kappa_s(z)^2$ dependence described above introduces some power dependence into the model, it does so in a very artificial manner. It ignores pump depletion effects and assumes that the longitudinal rate of change of the Stokes beam on the left and right hand sides of Equation (3.5) are different. The $\kappa_s(z)^2$ term on the right side is forced to assume the exponential form in Equation (3.7) while, on the left side, the rate of change is left unspecified. It was shown in the previous chapter that a more natural mathematical solution involves making no such assumption about $\kappa_s(z)^2$ and simply separating variables to solve the differential equation, though now with a $\kappa_p(z)^2$ derived from a plane wave model, that accounts for pump depletion.

The conclusions of the previous sections pointed out many of the relevant issues in modeling SBS phase conjugation. These included the relative performance of phase conjugate, fundamental, and random modal distributions, as well as the effects one encounters when varying fiber length and input pump power. While useful in laying the groundwork and getting a feel for the phenomena involved, these concerns are now left behind in favor of a more practical model output that can easily be compared to experimental observations.

One of the most common measurements of phase conjugate performance makes use of the design shown below in Figure (4.8). Consider a Gaussian input beam that is focused such that it is incident through a pinhole just large enough to give a high

transmission. After the pinhole, an aberrator is introduced to distort the beam and then another lens, or combination of lenses, is used to focus the distorted beam into the SBS active medium. Here we focus on a silica fiber waveguide as the nonlinear material. If a perfect phase conjugate is reflected, it will be distorted upon exit from the fiber, but will regain its Gaussian form after a second pass through the aberrator and will experience a 100% power transmission through the pinhole. If some other non phase-conjugate Stokes configuration is reflected, it will be further distorted after a second pass through the aberrator, and will experience a very low transmission through the pinhole. By taking the backscattered power after the pinhole and dividing by the power before the pinhole, one will find the 'phase conjugate fidelity,' F, a very common experimental measure of whether phase conjugation is present. A perfect phase conjugate would have $F = 1$, though this is unrealistically high in practice.
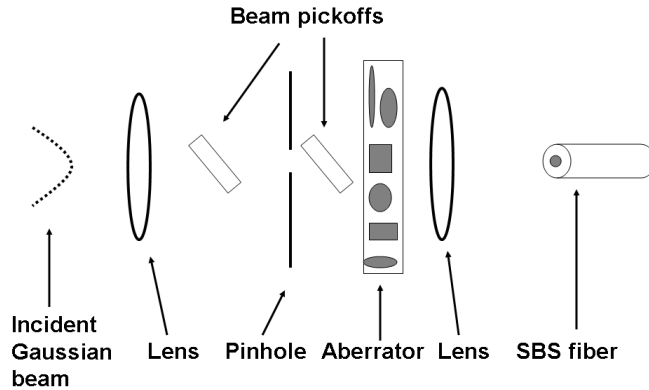
Figure 4.8.   A schematic of a pinhole experiment to measure phase conjugate fidelity. An incident Gaussian beam is focused through a pinhole, experiencing high transmission, and is distorted by an aberrator before being focused into a fiber which serves as the phase conjugating medium. A high quality phase conjugate will be 'cleaned up' upon a second pass through the aberrator and again experience high transmission through the pinhole, which can be measured by the two beam pickoffs.

So far, an 'in fiber' model has been described. That is, a certain starting pump input modal distribution, or 'speckle' pattern, is assumed at the front end of the fiber such that calculations about various backscattered Stokes beams can be made. To make predictions about fidelity, the model was expanded to include free space Fourier propagation. A starting Gaussian beam was focused through a thin lens, propagated through a pinhole, transmitted through a second thin lens, and propagated a certain distance to the fiber tip. Including an aberrator, as mentioned above, introduced modeling difficulties that are beyond the scope of this discussion. As an alternative, the aberrator was omitted but the resulting Gaussian beam was purposely focused off-center onto the fiber tip. Thus, multiple modes were excited in the fiber despite the 'clean' single-lobed incident beam. Even with the lack of an aberrator, this off-center focus thus preserves the pinhole power transmission as a measure of phase conjugate fidelity.

Once the incident beam was propagated through this simple optical system, and focused, off-center, onto the fiber tip, one must determine what fiber modes this electric field will excite. To do this, a simple algorithm was used whereby, with a random starting field, the product of the incident electric field and the fiber field was integrated in the transverse plane, with the amplitudes and the phases of the fiber field adjusted to maximize this integral. This algorithm serves as the 'link' between the free space Fourier propagation and the in-fiber model by translating a given free-space electric field distribution into the modal distribution of amplitudes and phases, A_p^i and ϕ_p^i, that are needed to proceed with calculations inside the fiber. As shown in
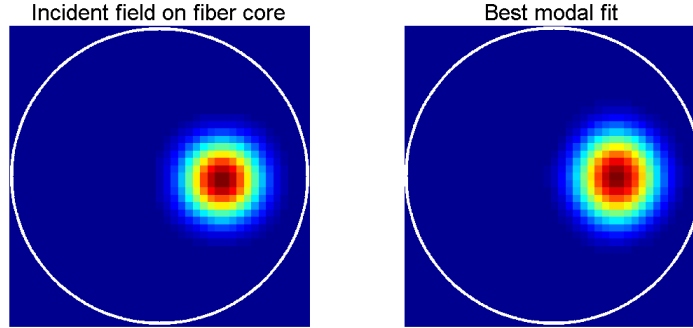
Figure 4.9.   A comparison of the Gaussian beam incident on a fiber core (left), and the closest match that the finite number of fiber modes can support (right). This example is for a 0.06 NA fiber with a 20 μm radius core (white outline) and with a focus 10 μm off-center onto the fiber tip. This fiber supports 12 LP modes.

Figure (4.9), this algorithm can produce excellent results where a certain distribution of modal amplitudes and phases inside the fiber can produce an irradiance pattern that very closely matches that incident from free space. It is very important that this match be as close as possible because a poor fit would produce a fidelity less than one even if a perfect phase conjugate were produced by the fiber. The pixel resolution in Figure (4.9) is only 1 μm. While a finer resolution is possible, it increases model computation time. For the weakly multimode fibers considered here, the irradiance pattern in the fiber varies slowly enough that this resolution is more than adequate. For the 0.13 NA fiber that is discussed later, a resolution of 0.5 μm was used.

The electric field fit shown in Figure (4.9) produced a distribution of the electric field amongst the 12 fiber modes of the 0.06 NA fiber as shown in Figure (4.10). Note that while a Gaussian beam is being coupled into the fiber, the fact that it is off-center implies that multiple higher order modes are excited, as desired. Knowing
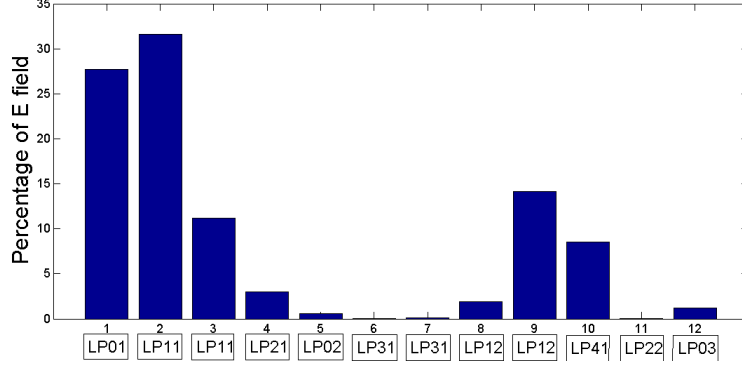
71

Figure 4.10. The distribution of the electric field amongst the various allowed modes of a 0.06 NA fiber with a 20 μm radius core when a Gaussian input beam is coupled in 10 μm off-center. Note some LP modes are repeated because they have a nondegenerate 90° rotation.

these modal amplitudes, as well as the corresponding phase shifts for each mode (not shown here), there is enough information to proceed with the in-fiber model.

The pump depletion portion of the model can now implement Equation (3.11), where the cosine terms can be simplified as described in Equation (3.20), $\kappa_p(z)^2$ is given by Equation (3.14), and $I_s(0)$ is found by the plane wave methods detailed in the previous chapter. The modal distribution found by the algorithm mentioned above, which produced the right-side of Figure (4.9), gives us the A_{pp}^{fq} and $\Delta\phi_p^{fq}$ terms. In previous sections, the $A_{ss}^{j\nu}$ and $\Delta\phi_s^{j\nu}$ terms were found by assuming a specific Stokes form, such as the fundamental LP_{01}, a phase conjugate, or random modal distributions. In this section, no such assumption about the Stokes is made. Rather, a perturbation algorithm similar to that mentioned above and used to produce Figure (4.9) is implemented to find the arrangement of Stokes amplitudes and phases that gives the maximum backscattered Stokes power from Equation (3.11). A flowchart detailing this algorithm is given in Figure (4.11).

Inputs:
Starting modal amplitudes / phases (for i^{th} mode): A^i_0 and ϕ^i_0
Amplitude / phase step-size: ΔA and $\Delta \phi$
Minimum improvement per iteration: Ω
For N modes

Start → $i = 1$ →

a | Find largest Stokes power of:
a) ϕ^i_0 b) $\phi^i_0 + \Delta\phi$ c) $\phi^i_0 - \Delta\phi$

b,c

Using same sign from b) or c) increment:
Find Stokes power of $\phi^i_0 \pm 2\,\Delta\phi$
Keep incrementing until power goes down, save resulting phase as ϕ^i_1

$\phi^i_0 = \phi^i_1$

Stop!
Output $\{A^i_1\}$ and $\{\phi^i_1\}$

$\{A^i_0\} = \{A^i_1\}$
$\{\phi^i_0\} = \{\phi^i_1\}$

No   Yes

a | Find largest Stokes power of:
a) A^i_0 b) $A^i_0 + \Delta A$ c) $A^i_0 - \Delta A$

b,c

Using same sign from b) or c) increment:
Find Stokes power of $A^i_0 \pm 2\,\Delta A$
Keep incrementing until power goes down, save resulting amplitude as A^i_1

$A^i_0 = A^i_1$

Find Stokes power for:
- $\{A^i_0\}$ and $\{\phi^i_0\}$ = P_0
- $\{A^i_1\}$ and $\{\phi^i_1\}$ = P_1

Is $P_1 / P_0 \geq \Omega$?

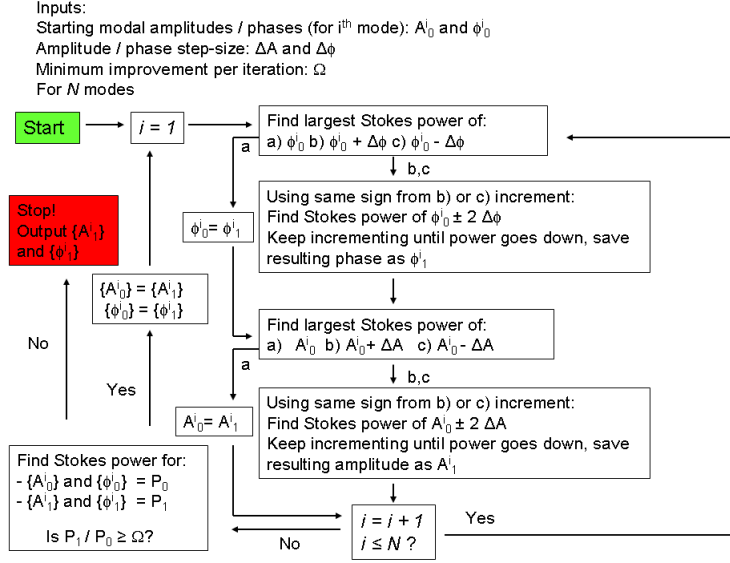No $i = i + 1$ $i \leq N$?   Yes

Figure 4.11.   A flowchart detailing the perturbation algorithm used to find the best performing Stokes configuration for a given pump input. Note that whenever an amplitude is adjusted, the whole set of amplitudes is re-normalized such that $\sum_i A_i^2 = 1$. All Stokes powers are calculated according to the plane wave pump depletion weighting method.

Implementing this algorithm, by following the steps in Figure (4.11) and using Equation (3.11) to calculate the Stokes power whenever needed will give, for a given pump input, the Stokes modal configuration that would maximize the backscattered power. An example output of this algorithm is given in Figure (4.12). One can clearly see that as the fiber under consideration is lengthened, the Stokes output looks less and less like the pump input. To put it more specifically, the phase conjugate fidelity drops.

Taking these predicted Stokes outputs, such as those pictured on the bottom row of Figure (4.12), and carrying out the same free space Fourier propagation, now in reverse back through the pinhole, one can easily find the phase conjugate fidelity by finding the power after and before the pinhole and taking the ratio. An optical
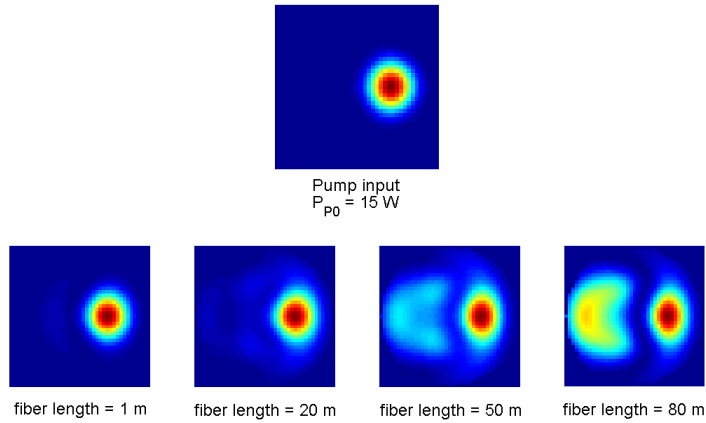
73

Figure 4.12. Predictions of the best performing Stokes modal configurations for a 40 μm core diameter, 0.06 NA fiber using the plane wave pump depletion weighting. The four outputs on the bottom row are all Stokes irradiance patterns as they exit the pump input end of the fiber.

setup similar to that of Figure (4.8) was used, except without an aberrator and with the pinhole placed at the Gaussian starting point on the left rather than in-between the lenses. A starting Gaussian beam radius of 20 μm was assumed with a pinhole of 30 μm radius, and the left and right lenses having focal lengths of 2 and 0.9 cm respectively. The resulting Gaussian was focused down onto the 0.06 NA fiber as shown in Figure (4.9), with the center of the fiber core shifted 10 μm away from the optical axis in one direction.

The resulting fidelity curve for this 0.06 NA fiber is shown in Figure (4.13), and compared to experimental data from the same fiber [21], and the fidelity predictions of Hellwarth [8]. As expected, the fidelity tends to drop with increasing fiber length in all cases. However, one can see that, though the assumptions made in this development have introduced some error, this model comes much closer to experimental data than
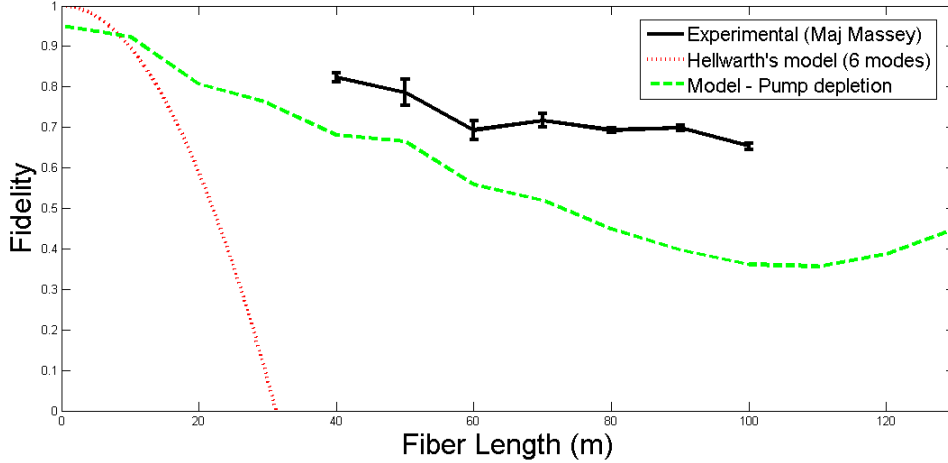
Figure 4.13. Modeled (dashed) vs experimental (solid) fidelity curves for a 40 μm core diameter, 0.06 NA fiber. For the pump depletion curve, the Brillouin gain was taken to be $5 * 10^{-11}$ m/W and the input pump power was $P_{P0} = 20$ W. Also shown is the prediction of Hellwarth's earlier model (dotted). Note that the curves do not account for whether the SBS threshold has actually been crossed.

the efforts of previous researchers, such as Hellwarth. Note that the Hellwarth fidelity

curve is obtained using Equation (2.36).

The increase in fidelity that starts at a length of 120 meters is at first counter-

intuitive. However, this effect arises because a large number of mode-sets accumulate

an integral number of 2π in phase at this fiber length. Recalling the reasoning that

led to Equation (3.20), and ignoring the case where $f = q$ and $j = \nu$, because this

leads to an infinite beat length, one can plot the length required for the $f = j$ and

$q = \nu$ propagation constant differences that appear in the cosine terms to accumulate

2π in phase. That is, one can plot $2\pi/(\Delta\beta_p^{fq} - \Delta\beta_s^{j\nu})$ for all the possible permutations

where $f = j$ and $q = \nu$. The results are shown in Figure (4.14).

There are very few data points beyond 140 meters, and so they are not plotted

in Figure (4.14). The mode-sets beat at distances that tend to cluster together, with
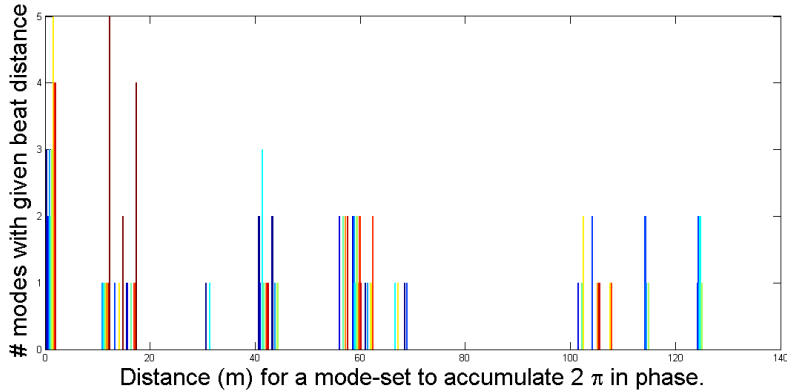
75

Figure 4.14.   An analysis of the distance required for the various modesets to accumulate 2π in phase in a 0.06 NA, $40\mu m$ diameter core fiber. The distances are found from $2\pi/(\Delta\beta_p^{fq} - \Delta\beta_s^{fq})$, where $\Delta\beta_{p,s}^{fq} = \beta_{p,s}^{f} - \beta_{p,s}^{q}$, and β is the longitudinal propagation constant.

the most noticeable groups being centered at approximately 15, 40, 60, and a large

group at approximately 105 meters. For a fiber length of 120 meters, nearly all of

these modes will accumulate close to an integral number of 2π in phase. As a fiber

is lengthened to 120 meters, the Stokes configuration that matches the pump near

the input will actually be, neglecting the pump depletion weighting, double weighted

because this 'speckle' pattern will nearly reproduce itself at the far end of the fiber.

It is worth noting that for fibers supporting a larger number of modes, this effect

quickly disappears as there are so many modal permutations that the clustering effect

disintegrates.

A very similar analysis to that presented above was carried out in Figure (4.15),

this time for a 0.13 NA fiber with a 20 μm core diameter. While the numerical aperture

is higher, the core diameter is halved, and so this fiber supports approximately the

same number of modes as the 0.06 NA, 40 μm core diameter fiber analyzed above.

However, the larger NA means that the propagation constants, β_i, for 'neighboring'

76

modes are more disparate, implying a more rapid evolution of the speckle pattern down the fiber. Thus, it was anticipated that the phase conjugate fidelity would drop more quickly as the fiber was lengthened. This behavior was indeed observed in Figure (4.15), where the fidelity has dropped roughly to its lowest value for a 25 meter long fiber, while it took a 100 meter 0.06 NA fiber for the fidelity to reach its minimum. Again, Hellwarth's predictions and the experimental data are shown, though this time additional model curves are given for the first two solutions considered in this thesis, the no pump depletion and decoupled no pump depletion cases. One can see that, as expected, the pump depletion fidelity curve comes closest to the experimental data and is the preferred solution from this model. Also note that the decoupled no pump depletion consistently predicts a very high fidelity regardless of length, because for an input pump power of 20 W the decaying exponential $\kappa_s(z)^2$ very heavily weights the front of the fiber, and thus the phase conjugate.

For this 0.13 NA fiber, the experimental data used a Gaussian that was input $7 \pm 2\mu m$ off-center, while the model used 5.5 μm because the electric field matching algorithm at the front fiber face could not produce a close match too far from the center of the fiber core. This means that a slightly different set of modes may have been excited experimentally than in the model. Also, the free space lens arrangements and pinhole size had to be adjusted in the model for both the 0.06 and 0.13 NA fibers to keep the free space beam from becoming too large, because the numerical Fourier propagation of a large beam with a 0.5-1 μm pixel resolution throughout was computationally prohibitive. Despite the different lenses, the spot-size on the fiber
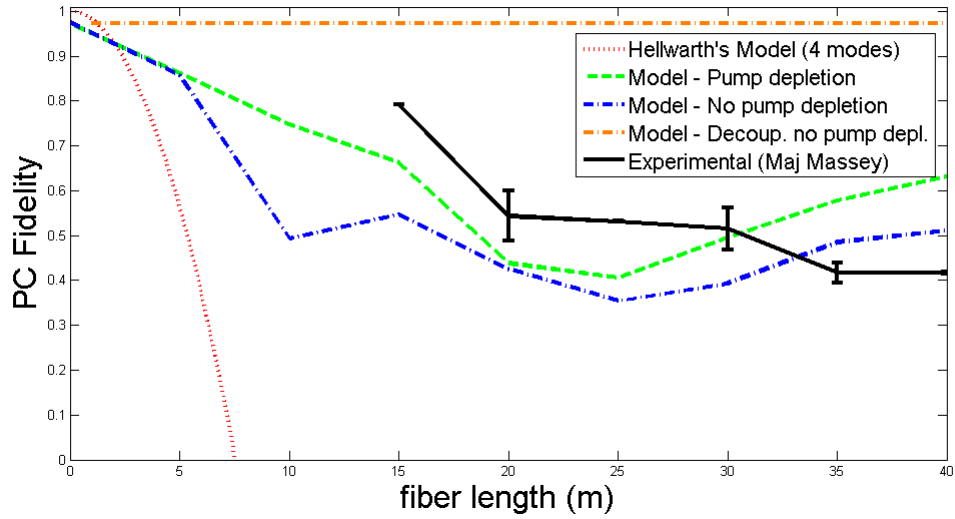
77

Figure 4.15.   Comparison of experimental (solid) vs predicted phase conjugate fidelity curves for a 20 μm core diameter, 0.13 NA fiber using the no pump depletion (dash-dot), decoupled no pump depletion (dash-dot), and pump depletion (dash) methods developed in this thesis. For the model, the Brillouin gain was taken to be $5 * 10^{-11}$ m/W and the input pump power was $P_{P0} = 20$ W. Also shown is the prediction of Hellwarth's earlier model (dot). Note that the curves do not account for whether the SBS threshold has actually been crossed.

tip was close to the experimental value and the pinhole in both model and experiment was just large enough to give a high transmission of the incident beam.

With these caveats in mind, the pump depletion model still makes a much more accurate prediction of the experimental data than previous efforts such as Hellwarth. Similarly to the 0.06 NA results in Figure (4.13), the model still tends to underpredict the experimental data, with an erroneous prediction of an increase in fidelity after a certain length of fiber. The underprediction error could be attributed to multiple causes. First, despite a best effort in model construction, the experimental conditions almost certainly do not match the model exactly, either in size of the coupled beam, or how far offcenter it was relative to the fiber core. This will change what

modes are excited, and thus the irradiance pattern along the fiber that determines the all-important Stokes gain. In addition, the electric field matching algorithm that produces plots similar to Figure (4.9) is not perfect, which means fidelities slightly less than one are predicted even for very short fibers, which gives a downward vertical off-set to the modeled fidelity curves. Even if these launching conditions and field fit were perfectly replicated, there are other effects such as mode-mixing or mode-dependent loss that could introduce error into the model.

Regarding the rise in fidelity at longer fiber lengths, this was attributed previously to a common mode-beat length for the majority of the modal permutations. If the current assumption of constant growth/decay across all the Stokes/pump modes is lifted and individual modal change rates are included, then an improved prediction would result. When coupling into the fiber, only a subset of the available modes are appreciably excited, as shown in Figure (4.10). Thus, only a subset of the modal combinations beat distances, represented in Figure (4.14), are important. When all the modes grow/decay at the same rate, these important contributors remain the same throughout the fiber, and will all accumulate an integral 2π in phase at the least common multiple of all their beat distances. However, if each mode grew or decayed at an independent rate, then the important subset of modal combinations in Figure (4.14) could change along the fiber as the modes evolved. That is, one would expect an increase in fidelity at the least common multiple of these mode beat distances, but these modal distances keep changing along the fiber as some modes decay, and others that may not have been initially appreciably excited can gain more power farther

into the fiber. The least common multiple then loses meaning, and may result in the elimination of this erroneous fidelity increase in the model.

Another interesting behavior, beam clean-up, was seen in many of the fiber simulations that used the Stokes performance maximizing algorithm of Figure (4.11). Traditionally, beam clean-up has been associated with graded index fibers, where the varying index across the core tends to favor modes with a high irradiance in the center [19]. As the fiber is lengthened, this discrimination against higher order modes becomes dominant, and the backscattered Stokes moves almost exclusively to the fundamental mode. However, the model predicts that a step index fiber can also exhibit beam cleanup, though now the modal discrimination occurs because of the launching conditions into the fiber, rather than being built directly into the fiber itself. This simultaneously makes step-index fiber beam cleanup more versatile, as well as haphazard.

As an example, consider the predicted backscattered Stokes irradiance patterns which were counterpropagated to obtain the modeled pump depletion fidelity curve (green dashed line) in Figure (4.15). A subset of these Stokes beams are shown in Figure (16(a)), where it it easily observed that, as the fiber is lengthened, phase conjugation gives way to beam cleanup to the LP_{11} rather than the LP_{01} mode. This occurs because for a longer fiber, the Stokes modal arrangement with the maximum overlap with the pump is the LP_{11} mode by itself, thus this mode alone experiences the maximum gain and dominates the output. While the pump input pictured at the top of Figure (16(a)) will excite multiple fiber modes, which will move at different

80
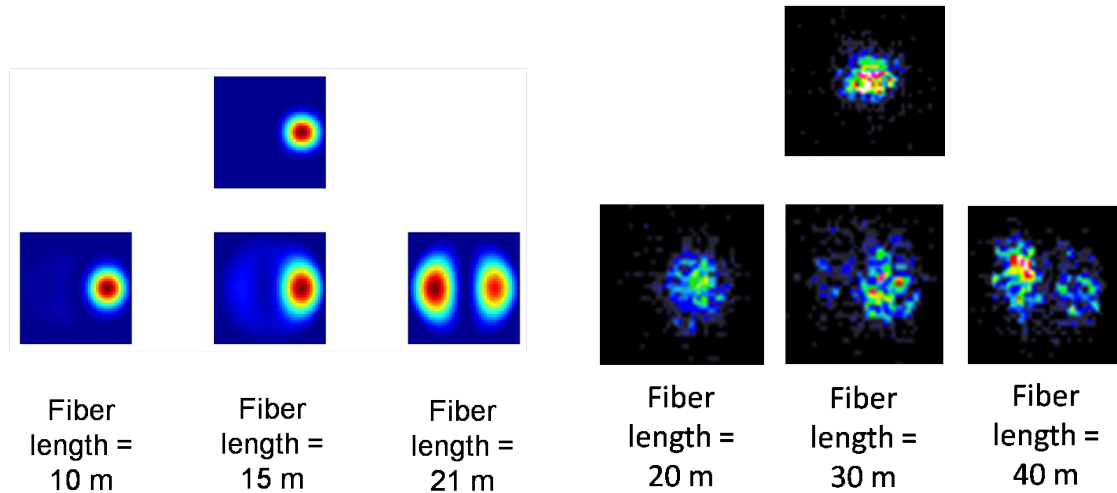
(a) Model predictions of the best performing Stokes modal configurations using the plane wave pump depletion weighting with $P_{P0} = 16$ W. Images are Stokes irradiance patterns as they exit the pump input end of the fiber.

(b) Experimental verification of transition from Stokes phase conjugation to beam clean-up to the LP_{11} mode with approximately 16 W input pump power

Figure 4.16. Modeled vs experimental irradiance patterns for LP_{11} beam cleanup in a step index fiber. A 0.13 NA fiber, with a 20 μm diameter core, was used in both model and experiment.

speeds and thus change the irradiance pattern, every so often the modes in the fiber will beat together, reproducing the single-lobed pattern seen at the beginning. Every time this happens, one half of the LP_{11} mode will have very high overlap with the pump, giving it the advantage mentioned above. This was confirmed experimentally, though at longer fiber lengths than the model predicts, as shown in Figure (16(b)) [21], with the length discrepancy likely due to the same sources of error mentioned above.

As was already mentioned, beam cleanup in step-index fibers is highly dependent on the launch conditions of the pump into the fiber. To test this, the Stokes maximizing algorithm was run on an input Gaussian beam that was coupled into a 0.13 NA, 20 μm fiber at varying distances from core center. As seen in Figure

81

(4.17), going from 3 to 4 μm off-center produced a dramatic change in Stokes beam cleanup from the LP_{01} to the LP_{11} mode. Thus, while this form of beam cleanup could potentially be very versatile in its ability to produce higher order modes, it is also haphazard in its sensitivity to launching conditions. Such higher order mode converters have attracted research interest from other groups, though their strategies typically employ the manufacture of specialty fibers at considerable cost [22], making this SBS-based conversion in a conventional step-index fiber of potential practical interest.
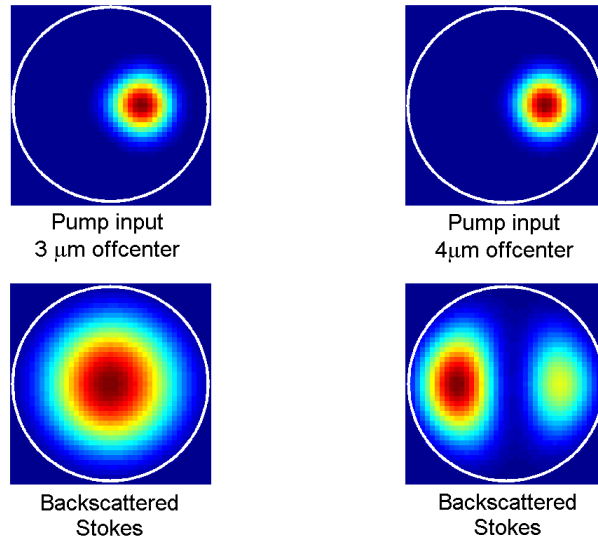

Figure 4.17.   An example of the importance of the launching conditions in step-index fiber beam cleanup. Launching a Gaussian just one micron farther off-center changes the Stokes output from LP01, to largely LP11. Model was run on a 20 m long, 0.13 NA, 20 μm diameter core fiber with a pump input power of 20 W.

The results shown here indicate Hellwarth's adapted relation, Equation (2.37), incorrectly requires extremely short fiber lengths for a decent phase conjugate. Taken at face value, such a design requirement might immediately lead to the abandonment

of a step-index fiber approach due to the extremely high power that would be required to excite SBS in such a short length. However, the numerical analysis conducted here, backed up by experimental evidence, indicates the requirements are much looser than it would initially appear. While the model still tends to underestimate the attainable fidelities, it comes much closer to experimental evidence, and represents a significant step forward in understanding the workings of these step-index fiber based SBS phase conjugate mirrors. Sources of error, especially the common modal longitudinal change term, Equation (2.32), were explored with their effect, such as the common modal beat distance leading to a rise in fidelity at long fiber lengths, explained. Lastly, the novel phenomenon of step-index fiber beam cleanup was predicted in the model, explained, and later experimentally verified [21].

V. Conclusion

Suggestions for Future Work

The work done here constitutes a significant step forward in the modeling capabilities of phase conjugation in a fiber waveguide. However, there are multiple improvements that would significantly increase the validity and applicability of the model.

The first and most important improvement would be to eliminate the assumption that all the modes of the fiber will grow or decay at the same rate. Referring back to Equation (2.25), the derivation previously proceeded by multiplying by $\vec{E}_s^*$, adding the complex conjugate form of the resulting equation, which put everything in terms of irradiances. The model was then constructed to assume that the various modal amplitudes, for example mode f of the Stokes beam A_s^f, all grew/decayed at the same rate. That is, the LP_{01} mode of the Stokes beam had to grow just as fast as the LP_{11} or LP_{32} modes. The LP_{01} mode of the pump would be depleted just as quickly as the LP_{21} mode. This was done for no other reason than it vastly simplified the analysis.

To eliminate this assumption, one could return to Equation (2.35). This form is essentially identical to that used by Hellwarth in his stationary perturbation theory approach in a rectangular waveguide. A relaxation method approach is recommended. As a starting point, assume a given pump input that is undepleted throughout the fiber, that is, A_{pp}^{ij} is known and unchanged in the entire waveguide. One could start

with a random Stokes modal distribution, as SBS starts from spontaneous noise, and implement Equation (2.35) to update the Stokes amplitudes throughout the fiber. An equation very similar to (2.35) exists for the pump amplitudes, and this form would be used to take the resulting Stokes amplitudes and alter the pump amplitudes, introducing depletion effects. This procedure is repeated until a steady state is reached. In this way, not only is each mode allowed to longitudinally change at its own rate, but pump depletion and Stokes growth effects are introduced 'naturally,' not by a construct such as a plane wave assumption.

As mentioned previously, attempts to implement this strategy have been made in the past, though they almost always used a free space SBS phase conjugate media, such as a compressed gas in a relatively large glass cylinder. This complicates the coupled SBS equations because the transverse Laplacian must be included due to the lack of a waveguide, and thus the above approach may be simpler in the case of a fiber. In addition, many of the attempts occurred 20 or more years ago and cited insufficient computer memory and processing power as a significant obstacle to success. These problems, obviously, may have self-resolved. Lehmberg was able to numerically model an SBS phase conjugate mirror in a waveguide using a similar method to that described here, but, for reasons he does not mention, limited his analysis to two dimensional waveguides, thus severely hampering the applicability of his work to practical devices [7]. Lehmberg, and multiple other authors, mention that the primary difficulty in solving the coupled differential equations is implementing conditions such that a stable solution is eventually reached [17].

This is the main, and potentially most exciting and far-reaching, improvement to the work considered here. However, other less arduous updates could also be made. The most obvious is to include the loss term in Equation (2.26b) in the analysis. Dropping this term for the short, silica fibers considered here is easy to rationalize as loss is usually negligible in these cases. However, chalcogenide fibers, which might be used for their much higher nonlinear gain coefficient, also exhibit much higher loss than silica at near infrared wavelengths, and including this term should be seriously considered if these wavelengths are to be used experimentally.

Another interesting experiment would be to repeat the fidelity curve calculations made in Figure (4.13) and (4.15), though with an aberrator introduced such that the beam being coupled into the fiber is not a Gaussian. This is how the majority of the phase conjugate experiments in the literature are conducted, but there was insufficient time to work out the modeling difficulties for this thesis. It was found that introducing a random number generated pattern for an aberrator produced a beam with very high spatial frequency content, which introduced high loss when being coupled into the fiber. When a 'smoothing' routine was introduced to the modeled aberrator, whereby each pixel was adjusted to the average of its neighbors, the problem lessened but was still present.

An aberrator is needed that introduces some sort of distortion, but does not vary extremely quickly across the transverse plane. One approach that held promise was to use a short segment of multimode fiber, of the same type as the SBS generating fiber, that would have several modes excited and thus output a non-Gaussian, 'aberrated,'

intensity pattern. This intensity would be Fourier propagated through free space and focused down onto the phase conjugating fiber. As the fibers are of the same type, they possess the same set of modes, and thus one can expect that the coupling loss into the second fiber would be low. If a true phase conjugate was generated, the short aberrating fiber would clean up the backscattered beam, but otherwise the beam would remain distorted.

Lastly, while the model uses the SBS threshold in terms of the longitudinal weighting term $\kappa_p(z)^2$, the fidelity curves make no mention of whether, at a certain power and fiber length, the backscattered power will actually be appreciable. Thus, even though the fidelity for a 5 meter device at 5 W may be high, such a device will be well below threshold and there will be no stimulated scattering. It would be useful to build some estimation of threshold into the model and plot only those points that actually exceed a user-defined SBS reflectivity coefficient. Even if the threshold was estimated from a plane-wave model, it would still be useful for a rough estimation.

Summary of Work and Results

A model was constructed to numerically analyze SBS phase conjugation in multimode step index fibers. Specifically, the goal was to determine how variables such as fiber size, numerical aperture, length, and input pump power affected the Stokes output. Multiple specific test cases were analyzed.

First, the no pump depletion case was considered, as it was the most simple. An analytic form of the effective SBS gain was obtained, and this form was used to

see how the phase conjugate Stokes performed compared to the fundamental mode, random Stokes modes, and to $zPC \neq 0$ phase conjugate patterns that occured within the fiber. As there was no pump depletion, all portions of the fiber were weighted equally. This accounted for the observed averaging effects that led to all Stokes configurations giving increasingly similar gains as the fiber was lengthened. Even this rudimentary model correctly predicted, as shown in Figure (4.2), that step index fibers do not generally give beam cleanup to the fundamental mode, except for special launching conditions. A comparison of different phase conjugate forms, Figure (4.3), as well as random Stokes configurations, Table (4.1), reinforced this averaging trend at longer fiber lengths.

Second, the decoupled no pump depletion solution was implemented. It was decoupled in that the $\kappa_s(z)^2$ term on the right side of Equation (3.5) takes an exponential form, while the $\kappa_s(z)^2$ on the left side, which is hidden in $P_s(z)$, is left unspecified. This simple exponential form for $\kappa_s(z)^2$ still yielded a closed form solution, though now it was for the Stokes power, not the gain. This difference yielded no problems in practice, as all the analysis involved taking the ratio and looking for qualitative patterns rather than absolute values. For low pump powers, the weighting effect was marginal and the resulting data was very similar to the simple no pump depletion case. For higher input pump powers, the weighting clearly showed its effect in multiple ways. In Figure (4.4), the phase conjugate was clearly favored over the LP_{01} mode, even at long fiber lengths. As one zPC form of the phase conjugate was compared to another in Figure (4.5), the dominant effect was observing that as

the pump power increased, the $zPC = 0$ m form increasingly dominated all other options. For the random Stokes modal data in Table (4.2) and Figure (4.6), the best performers at longer fiber lengths and higher pump powers clearly bore some resemblance to the pump input, while lowering the pump power resulted in the highest gain corresponding to a Stokes with little resemblance to the pump.

Finally, the pump depletion case was analyzed. The $\kappa_s(z)^2$ term was left unspecified, and treated equally on both sides of the differential equation. However, rather than setting $\kappa_p(z)^2 = 1$, as was done in the two previous cases, a plane wave model was used to find what $\kappa_p(z)^2$ would be in a single-mode fiber, and then this weighting was applied equally to all the modes the pump excited inside the fiber. This was done for simplicity. Implementing a more rigorous analysis, as detailed above in the future work suggestions, would be the most far-reaching improvement to the model. However, even with this simplification, interesting results were obtained that appear to match the available experimental data.

Rather than repeating the same comparisons that were considered for the two no pump-depletion cases, here the model was geared towards producing curves of phase conjugate fidelity as a function of fiber length, which matches what is most easily measured experimentally. To do this, Fourier free space propagation was considered of an incident Gaussian through a pinhole and incident off-center on a fiber, as shown in Figure (4.8), though without an aberrator. The incident field was then run through a matching algorithm, whereby the overlap integral of the free-space electric field was

89

maximized as the field inside the fiber was adjusted. For incident Gaussians, this often produced very good results, as seen in Figure (4.9).

From here, the 'in-fiber' model took over and used the algorithm detailed in Figure (4.11), with the gain being calculated by Equation (3.11), to predict the output Stokes beam. These output beams were then free-space Fourier propagated back through the pinhole, with the ratio of powers after and before the pinhole giving the fidelity curves for various fibers seen in Figures (4.13) and (4.15). The fidelity predictions for from this model proved to be much closer to experimental data than previous theoretical efforts. The erroneous prediction of an increase in fidelity at longer fiber lengths was attributed to a common mode-beat effect that likely has its origins in the simplifying assumption of Equation (2.32).

Furthermore, it was shown, in Figures (16(a)-16(b)), that for long fibers and certain off-center pump coupling conditions, beam cleanup can be observed. While this is more versatile than graded-index fiber beam cleanup, which favors only the LP_{01} mode, it is also more haphazard as the specific 'cleaned mode' is very sensitive to the launch point into the fiber, as seen in Figure (4.17).

The numerical model constructed for this thesis has thus been successful in explaining previously observed phenomena, as well as making accurate predictions that were later born out by experimental evidence. It could prove a valuable tool for researchers trying to build SBS phase conjugate mirrors from step-index fibers, especially when trying to make design decisions about fiber NA, core size, length, and

required input pump power. By enabling near-aberration free high power amplifiers or coherent beam combination, these mirrors could be of great utility in military applications simultaneously requiring high power and good beam quality.

Bibliography

1. T.H. Maiman. Stimulated optical radiation in ruby. *Nature*, 187:493–494, 1960.

2. David M. Pepper. Nonlinear optical phase conjugation. *Optical Engineering*, 21(2):156–183, 1982.

3. David M. Pepper. Applications of optical phase conjugation. *Scientific American*, pages 74–83, January 1986.

4. B.Y. Zel'Dovich. Connection between the wave fronts of the reflected and exciting light in stimulated mandel'shtem-brillouin scattering. *Journal of Experimental and Theoretical Physics Letters*, 15:109, 1972.

5. G.G. Kochemasov and V.D. Nikolaev. Reproduction of the spatial amplitude and phase distributions of a pump beam in stimulated brillouin scattering. *Soviet Journal of Quantum Electronics*, 7:60–63, 1977.

6. B.Y. Zel'Dovich and T.V. Yakovleva. Small-scale distortions in wavefront reversal of a beam with incomplete spatial modulation. *Soviet Journal of Quantum Electronics*, 10:181–186, 1980.

7. R.H. Lehmberg. Numerical study of phase conjugation in stimulated brillouin scattering from an optical waveguide. *Journal of the Optical Society of America*, 73(5):558–566, 1983.

8. R.W. Hellwarth. Theory of phase conjugation by stimulated scattering in a waveguide. *Journal of the Optical Society of America*, 68(8):1050–1056, 1978.

9. Amnon Yariv. *Optical Electronics*. Holt, Rinehart and Winston, Inc., Philadelphia, Pennsylvania, 1991.

10. Mark A. Heald and Jerry B. Marion. *Classical Electromagnetic Radiation*. Thomson Learning, London, United Kingdon, 1995.

11. D. Gloge. Weakly guiding fibers. *Applied Optics*, 10:2252, 1971.

12. Bahaa E.A. Saleh. *Fundamentals of Photonics*. John Wiley Sons Inc., Hoboken, New Jersey, 2007.

13. Timothy H. Russell. *Laser Intensity Scaling through Stimulated Scattering in Optical Fibers*. PhD thesis, Air Force Institute of Technology, December 2001.

14. Robert W. Boyd. *Nonlinear Optics*. Academic Press, Inc., San Diego, California, 1992.

15. Partha P. Banerjee. *Nonlinear Optics*. Marcel Dekker, Inc., New York, New York, 2004.

16. Timothy H. Russell, Brent W. Grime, Thomas G. Alley, and Won B. Roh. *Stimulated Brillouin scattering beam cleanup and combining in optical fiber*, chapter 7. Research, Kerala, India, 2007.

17. Eugene J. Sigal. SBS modeling - status and assessment. Technical report, W.J. Schafer Associates, Inc., October 1989.

18. B. Y. Zel'dovich, N.F. Pilipetskii, and V.V. Shkunov. Phase conjugation in stimulated scattering. *Soviet Physics Uspekhi*, 25(10):713–737, 1982.

19. L. Lombard, A. Brignon, J.-P. Huignard, and E. Lallier. Beam cleanup in a self-aligned gradient-index brillouin cavity for high-power multimode fiber amplifiers. *Optics Letters*, 31(2):158–160, 2006.

20. H.J. Eichler, J. Kunde, and B. Liu. Quartz fibre phase conjugators with high fidelity and reflectivity. *Optics Communications*, 137:327–334, 1997.

21. Steven M. Massey. written communication, January 2008.

22. A. Witkowska, S.G. Leon-Saval, A. Pham, and T.A. Birks. All-fiber LP11 mode convertors. *Optics Letters*, 33(4):306–308, 2008.

REPORT DOCUMENTATION PAGE

1. REPORT DATE *(DD-MM-YYYY)*	2. REPORT TYPE	3. DATES COVERED *(From - To)*

4. TITLE AND SUBTITLE	5a. CONTRACT NUMBER
	5b. GRANT NUMBER
	5c. PROGRAM ELEMENT NUMBER

6. AUTHOR(S)	5d. PROJECT NUMBER
	5e. TASK NUMBER
	5f. WORK UNIT NUMBER

7. PERFORMING ORGANIZATION NAME(S) AND ADDRESS(ES)	8. PERFORMING ORGANIZATION REPORT NUMBER

9. SPONSORING/MONITORING AGENCY NAME(S) AND ADDRESS(ES)	10. SPONSOR/MONITOR'S ACRONYM(S)
	11. SPONSOR/MONITOR'S REPORT NUMBER(S)

12. DISTRIBUTION/AVAILABILITY STATEMENT

13. SUPPLEMENTARY NOTES

14. ABSTRACT

15. SUBJECT TERMS

16. SECURITY CLASSIFICATION OF:			17. LIMITATION OF ABSTRACT	18. NUMBER OF PAGES	19a. NAME OF RESPONSIBLE PERSON
a. REPORT	b. ABSTRACT	c. THIS PAGE			
					19b. TELEPHONE NUMBER *(Include area code)*